ACS OMEGA

Open Access

http://pubs.acs.org/journal/acsodf

Article

Cysteine as an Eco-Friendly Anticorrosion Inhibitor for Mild Steel in Various Acidic Solutions: Electrochemical, Adsorption, Surface Analysis, and Quantum Chemical Calculations

Hanaa. M. Elabbasy,* Arafat Toghan,* and Hend. S. Gadow*

Cite This: *ACS Omega* 2024, 9, 13391−13411

Read Online

ACCESS | Metrics & More | Article Recommendations | Supporting Information

ABSTRACT: The corrosion of iron in acidic environments has a negative impact on global industry. Herewith, the inhibitory effect of cysteine (Cys.) on mild steel (MSL) corrosion in different acidic solutions (1 M HCl, 1 M H_2SO_4, and 1 M H_3PO_4) was investigated through weight loss, potentiodynamic polarization (PDP), electrochemical impedance spectroscopy, scanning electron microscopy (SEM), and theoretical calculations. The measurement results indicated that the adsorption of Cys. molecules on the metal surface caused corrosion inhibition. As a result, a protective layer or insoluble compound, or both, is obtained, blocking the active sites, preventing corrosion. The effectiveness (IE %) of the Cys. was enhanced by increasing concentration and lowering temperature. The maximum IE % of inhibition at 1×10^{-2} M of Cys. obtained are 97.3, 89.7, and 84.4% in HCl, H_3PO_4, and H_2SO_4 solutions, respectively. At the same inhibitor concentration, the double-layer capacity decreased, and the charge-transfer resistance increased from 17.17 to 188.5, 3.564 to 31.91, and 1.325 to 8.715 Ω cm^2 in HCl, H_3PO_4, and H_2SO_4 solutions, respectively. Adsorption and PDP studies confirmed that it obeys the Langmuir adsorption isotherm and acts as a mixed-type inhibitor of physicochemical nature. The corresponding thermodynamic and kinetic parameters were also calculated and discussed. Moreover, the inhibitory effect on the surface was inspected by SEM. The findings demonstrated that the order of IE % using Cys as anticorrosion agent for MSL is HCl > H_3PO_4 > H_2SO_4 solutions.

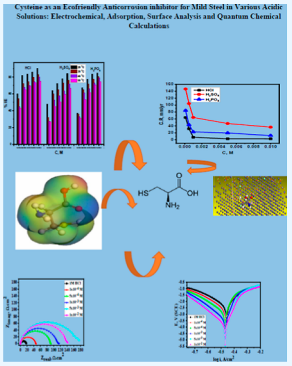

1. INTRODUCTION

Iron and its alloys are used as building materials in a range of industrial uses, including the petroleum, electricity, and chemical industries, due to its superior mechanical durability, ease of processing, and low production cost.[1,2] Due to its high mechanical qualities and thermal conductivity, mild steel (MSL) is one of the metallic materials used for a variety of purposes, including the production of drilling equipment, storage tanks, reactors, and other devices.[3] Hydrochloric acid is generally used in the pickling processes of metals and alloys. The corrosion of steel in such environments and its inhibition constitute a complex problem of processes.[4] Sulfuric acid is almost as frequently used for metal pickling as hydrochloric acid, but it does not evaporate, hence it is typically employed for pickling at high temperatures. Phosphoric acid (H_3PO_4) is widely used in the production of fertilizers and surface treatment of steel such as chemical and electrolytic polishing or etching, chemical coloring, removal of oxide film, phosphating, passivating, and surface cleaning.[5] A multitude of processes expose steel to corrosive conditions, including etching, acid pickling, acid descaling, acid cleaning, and oil-well acidification.[6,7] One of the most practical and economical ways to reduce/control corrosion rates and increase the lifespan of metallic products is to utilize inhibitors.[8−11] A chemical agent used sparingly to minimize the amount of time that metallic materials are exposed to corrosive conditions is known as an inhibitor. When present in the corrosive medium at an appropriate concentration, inhibitors, which function at the interface of the corrosive media and the metal surface, slow the pace of metal corrosion. Numerous organic compounds with long carbon chains or aromatic rings including hetero atoms like nitrogen, oxygen, sulfur, and phosphorus have been used as potential corrosion inhibitors in acid solutions.[12−15] The physicochemical characteristics of the inhibitor, such as the functional groups, steric factors, aromaticity, electron density at the donor atoms, the π-orbital nature of donating electrons, the structure of the molecule, the corrosion environment, and the charge and nature of the metal, are what primarily determine the inhibitor's ability to inhibit.[16,17] Amino acids are naturally occurring, biodegradable, relatively inexpensive, and synthesized with a high purity level of greater than 99%. They also represent a family of nontoxic, water-soluble chemical compounds.[18] The corrosion of different metals can be controlled by Cysteine (Cys.), which has the amino group [NH_2], the carboxyl group [COOH], and the thiol group [SH]. These functional groups enable strong adsorption

Received: December 30, 2023
Revised: February 15, 2024
Accepted: February 21, 2024
Published: March 7, 2024

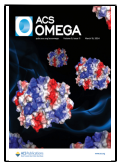

on the metal surface and protect it. Particularly, the oxygen atom of the carboxyl group, the nitrogen atom of the amino group, and the sulfur atom of the thiol group are its three coordination partners with metals.[18−21] It serves as the primary protein in skin, hair, and nails and is the building block of collagen supplements. It is also utilized as an ingredient in food, medicine, and personal care items.[22] Cys. has a limited potential for bioaccumulation in aquatic species and is a safe, easily biodegradable alternative to the frequently used amine absorption solvents and inorganic corrosion inhibitors. Based on rat oral testing, Cys. has a fatal dosage (LD50) value that is higher than that of amine solvents (MEA, DEA, and MDEA), and it is significantly higher than that of inorganic inhibitors [nickel(II) sulfate hexahydrate, copper carbonate, sodium metavanadate, and vanadium pentoxide].[23,24] After 28 days, almost 98% of Cys. may be broken down in an aerobic environment. This rate of biodegradation is quicker than MDEA but comparable to MEA.[23−25] Cys. has a lower bioaccumulation than MEA, DEA, and MDEA, as indicated by the log partition of Cys. in octanol/water (pow). Because of their strong propensity for bioaccumulation, sodium metavanadate, copper carbonate, vanadium pentoxide, and nickel(II) sulfate hexahydrate are hazardous to aquatic life.[24] Cysteine has the ability to control the corrosion of various metals. Generally, Cys. is a very interesting amino acid that contains amino group [$-NH_2$], carboxyl group [−COOH], and thiol group [−SH]. It can coordinate with metals through the nitrogen atom, oxygen atom of the carboxyl group and sulfur atom of thiol group. Cys. has been used to prevent the corrosion of a wide variety of metals in various environments acidic.[26−35]

In light of this, the study aims to explore and compare the mechanism of Cys. in preventing corrosion of MSL in different acidic media under the same conditions, including hydrochloric acid, sulfuric acid, and phosphoric acid solutions at temperatures ranging between 25 and 55 °C, using chemical, electrochemical, and surfactants. In addition, quantum chemistry and molecular dynamics calculations have been applied. The results demonstrate that Cys. (Mol. formula = $C_3H_7NO_2S$ and Mol. weight = 121.16 g mol^{-1}) may act as a powerful corrosion inhibitor of MSL under different corrosion conditions. The chemical structure of Cys. are shown in Figure 1.

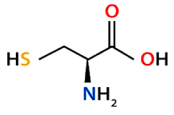

Figure 1. Chemical structure of Cys.

2. EXPERIMENTAL SECTION

2.1. Materials and Solutions. The MSL used in this study has the following composition (% wt): Fe = 99.22, C = 0.21, Si = 0.38, P = 0.09, S = 0.05, and Mn = 0.05. Cys. was obtained from Sherman Chemicals company. Prior to the measurements, the MSL samples were washed with bidistilled water and acetone after it progressively polished with emery paper up to 1000 grade. By diluting the concentrated acids with distilled water, various corrosive media were prepared for 1 M solutions of HCl, H_2SO_4, and H_3PO_4. A stock solution of Cys. inhibitor (0.1 M) was prepared by dissolving the appropriate amount in distilled water. From that solution, the desired concentrations (1×10^{-4}, 5×10^{-4}, 1×10^{-3}, 5×10^{-3}, and 1×10^{-2} M) were obtained by dilution using double distilled H_2O.

2.2. Weight Loss Method. MSL samples with dimensions of 2 × 2 × 0.1 cm were prepared and weighed accurately. They were then suspended in solutions of 100 mL of the acid corrosive media (1 M HCl, 1 M H_2SO_4, and 1 M H_3PO_4) without and with different concentrations of the Cys. for different immersion time (30, 60, 90, 120, 150, and 180 min), after which the samples were removed and handled in accordance with the procedure approved in ASTM designation G1−90.[36] For these samples, the following measurements of the average weight loss (WL) at a specific time were made

$$\Delta W = W_o - W_1 \tag{1}$$

The weights of the MSL coupons before and after soaking are W_o and W_1, respectively. The following formulas can be used to calculate the metal surface coverage (θ) and inhibitory efficiency (% IE)[37]

$$\%\ \mathrm{IE} = \theta \times 100 = \left(1 - \frac{\Delta W_{inh}}{\Delta W_{free}}\right) \times 100 \tag{2}$$

where WL (mg) without and with Cys. are denoted by W_{free} and W_{inh}, respectively. The following formula can be used to calculate the corrosion process rate (k)[38]

$$k = \frac{\Delta W}{AT} \tag{3}$$

where t is the immersion period in minutes and A is the sample area in cm^2.

2.3. Electrochemical Measurements. Computer controlled Gamry instrument Potentiostat/Galvanostat/ZRA (REF 600, model Gamry, Warminster, PA, USA), and software (Gamry's EIS300 program and DC105) was used for performing all electrochemical measurements. A three-electrode electrochemical cell consisting of a working electrode (MSL) with an active surface area of 1 cm^2, a counter (Pt wire), and a reference electrode (SCE), was prepared according to the standard process for electrochemical experiments.[39] In each run, collection of electrochemical data points began after reaching a steady state potential (OCP) of approximately 30 min. At a scan rate of 0.1 mV s^{-1}, the potentiodynamic polarization (PDP) curves were initiated from −0.6 to 0 V (vs SCE) over the corrosion potential ($Ec_{orr.}$). Thereafter, eq 4 was applied to estimate the surface coverage (θ) and inhibition efficacy (% IE), and eq 5 for the corrosion rate (C.R) calculation as follows.[40]

$$\%\ \mathrm{IE} = \theta \times 100 = \left[1 - \frac{i_{corr(inh)}}{i_{corr(free)}}\right] \times 100 \tag{4}$$

$$\%\ \mathrm{C.R\ (mm/year)} = 3270 \times \left[i_{corr} - \frac{EW}{D}\right] \tag{5}$$

where EW is the equivalent weight of MSL (g), D is the density of MSL (g cm^{-3}), and $i_{corr(free)}$ and $i_{corr(inh)}$ are the corrosion current densities (A cm^{-2}) without and with Cys., respectively.

For electrochemical impedance spectroscopy (EIS) experiments, AC signals with 5 mV peak-to-peak amplitude at corrosion potential and frequencies between 100 kHz and 0.01 Hz were used. Using the Gamry Echem Analyst program, all impedance parameters were fitted to the proper equivalent circuits (ECs). Using the EIS data, % IE can be calculated as follows

https://doi.org/10.1021/acsomega.3c10522
ACS Omega 2024, 9, 13391−13411

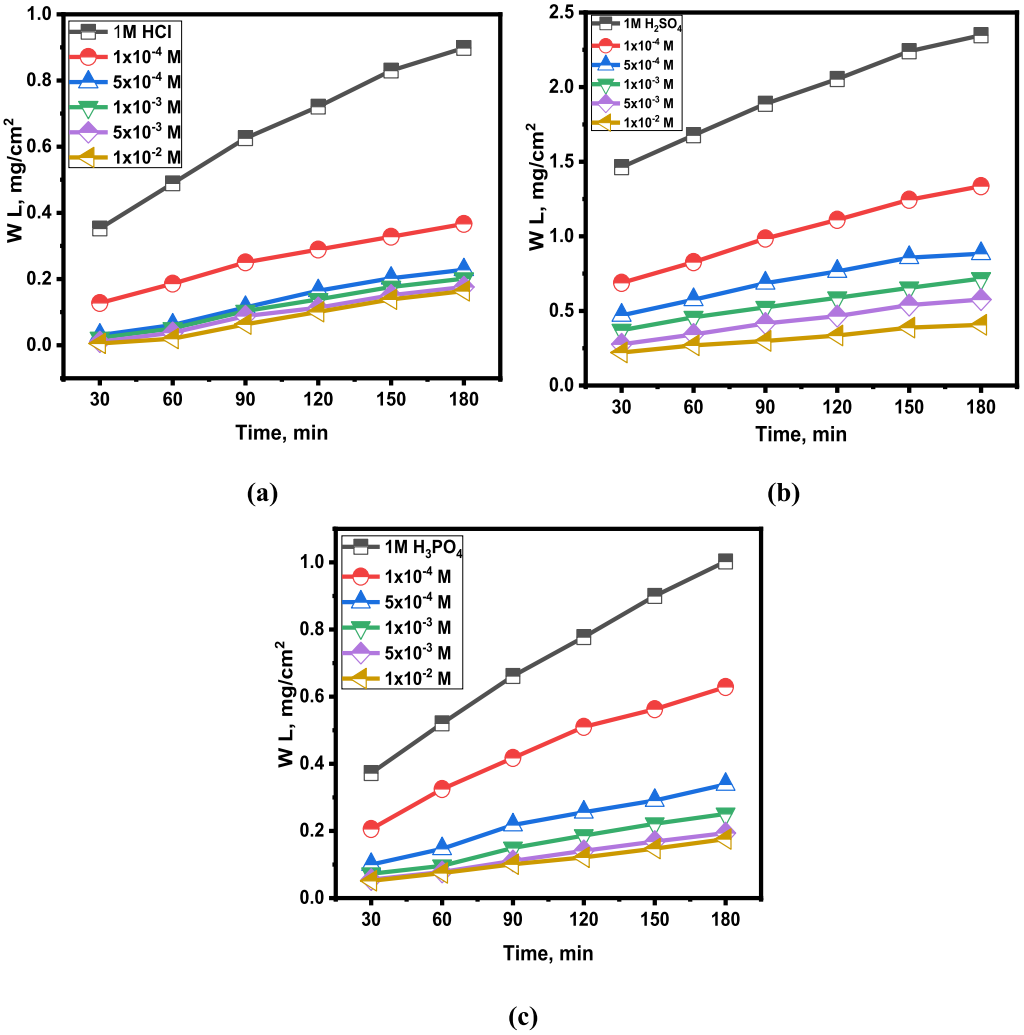

Figure 2. Effect of Cys. concentration variation on the MSL corrosion in a 1 M of: (a) HCl, (b) H_2SO_4, and (c) H_3PO_4 at 25 °C.

$$\%\ \mathrm{IE} = \theta \times 100 = \left[1 - \frac{R_{ct(free)}}{R_{ct(inh)}}\right] \times 100 \tag{6}$$

The charge-transfer resistances without and with the inhibitor are $R_{ct(free)}$ and $R_{ct(inh)}$, respectively.

2.4. Surface Analysis. A JEOL T-200 (x500) scanning electron microscopy (SEM) was used to examine the MSL surfaces. The samples were immersed for 24 h in one of three corrosive acidic solutions (1 M HCl, 1 M H_3PO_4, and 1 M H_2SO_4) without and with Cys. (1×10^{-2} M).

2.5. Theoretical Studies. *2.5.1. Computed Quantum Chemistry.* The compound was looked up using Material Studio's DMol3 module (type 7.0). The general gradient approach (GGA) was merged with a core group of beck one substitutable relationship functions (BOP) and double-digit polarization in the DMol3 item, and solvent influence were managed using COSMO control. The two techniques were used to derive the following chemical characteristics: electronegativity (χ), smoothness (σ), chemical potentials (μ), and global hardness (η), as definite in the next equations.[41,42]

$$I, \text{(ionization potential)} = -E_{HOMO} \tag{7}$$

$$A, \text{(electron affinity)} = -E_{LUMO} \tag{8}$$

$$\mu = -\chi \tag{9}$$

$$\mu = \frac{(E_{LUMO} + E_{HOMO})}{2} \tag{10}$$

$$\eta = \frac{\Delta E}{2} = \frac{(E_{LUMO} - E_{HOMO})}{2} \tag{11}$$

$$\sigma = \frac{1}{\eta} \tag{12}$$

$$\omega, \text{(electrophilicty index)} = \frac{\mu^2}{2} \tag{13}$$

$$\varepsilon, \text{(nucleophilicity index)} = \frac{1}{\omega} \tag{14}$$

The proportion of transported electrons (ΔN) was calculated using the following equation, the global hardness, and electronegativity parameters

$$\Delta N = \frac{(\chi_{Fe} - \chi_{inh})}{2(\eta_{Fe} + \chi_{inh})} \tag{15}$$

The signs χ_{in} and χ_{Fe}, respectively, symbolize the final electronegativity values for Cys. and MSL. Based on the studies from several publications, the electronegativity of Fe is 4.28 V/

https://doi.org/10.1021/acsomega.3c10522
ACS Omega 2024, 9, 13391−13411

mol, and its stiffness is 0 V/mol.[43−45] The local reactivity of a molecule was finished using Fukui function accounting as well. For electrophilic and nucleophilic assaults by inhibitor molecules, Fukui+ and Fukui, respectively, are the favored targets.

2.5.2. Molecular Dynamics Modeling. This work utilized the adsorption locator module from Material Studio 7.0 for molecular dynamic modeling.[46] The adsorption finder can locate Cys. molecules by imitating chemical particles adhering to a MSL surface. As the investigated Cys. compound has been shown to lessen the corrosion of MSL under acidic circumstances, it is important to investigate the adsorption of neutral and protonated inhibitor molecules in the presence of water molecules, which compete for active sites on the surface of iron (110). This was accomplished by adding 250 water molecules, 10 hydronium ions, and 10 chloride ions as coadsorbates. Using the imitation box (32.27, 32.27, 50.18 Å), the MSL (110) was extended across areas with periodic boundaries, passing a random fence for each result to resemble an interface model piece. The particle energy of the Cys. compound was enhanced using a typical simulation engine. After a 20° angle, a supercell formed, increasing the area of MSL (110), which also changed its spin. There was a thick vacuum coating covering the MSL's surface (110).[47] The atomic simulation studies (COMPASS) mimicked the adhesion of Cys. molecules to the surface of MSL by using the molecular potential of the ideal molecular stage (110). In order to examine the inhibitory strength of the investigated inhibitor as well as the structure of adsorption, Monte Carlo simulations were utilized to examine the likelihood of the inhibitor molecules adhering to the surface of iron (110).[48]

3. RESULTS AND DISCUSSION

3.1. Weight Loss. WL experiments for MSL were conducted in the three acidic media at different immersion times (t) and

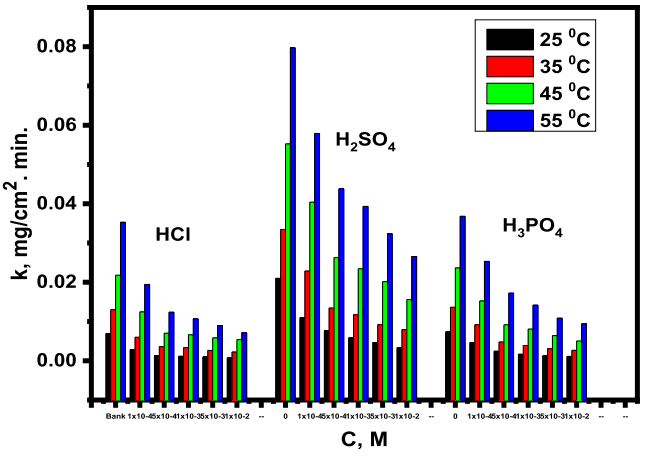

Figure 3. Corrosion rate vs conc. of Cys. for corrosion of MSL in a 1 M solution of HCl, H_2SO_4, and H_3PO_4 at different temperatures.

temperatures (25−55 °C) in absence and existence of Cys. inhibitor (1×10^{-4} to 1×10^{-2} M). Figure 2 shows the correlations between WL and t using different acids without and with various inhibitor concentrations at 25 °C. The average values of the corrosion rate and percent IE for Cys. on MSL are also shown in the ESI (electronic Supporting Information), Tables (S1−S3). According to Tables (S1−S3), the corrosion rates decrease, and percent IE rose with increasing Cys. concentration while the temperature stayed the same for all corrosive media. This is explained by the fact that the Cys. molecules enhanced adsorption coverage on the MSL with increasing its concentrations, inhibits the MSL dissolving degrees in the acid media. The results show that the examined Cys. compound is effective MSL corrosion inhibitor in all acids studied.

3.1.1. Effect of Temperature. The effect of varying temperatures (25, 35, 45, and 55 °C) in the three-acid media on k (corrosion rate) and % IE for MSL without and with different concentrations of Cys. is displayed in Figures 3 and 4, respectively. The results are summarized in Tables (S1−S3) in the Supporting Information. The process was also further investigated and is shown in Figures S1−S12 in the Supporting Information. The figures show that an increase in % IE results from a decrease in k value with increasing Cys. concentration. This is often because the degree of adsorption and the resulting surface covering increase as the concentration of Cys. does.[49] According to Figures 3 and 4 the k of MSL without and with Cys. in 1 M H_2SO_4 > k in 1 M H_3PO_4 > k in 1 M HCl, and the order of this increasing is opposite to the order of increasing percent IE in different acids solutions, where % IE in HCl > H_3PO_4 > H_2SO_4. On the basis of physical adsorption, it is possible to explain why inhibition efficiency values decline with increasing temperature (see Tables S1−S3) and gradually growth with increasing Cys. molar concentration.[50] WL measurements at different temperatures (25−55 0C) with and without the Cys compound were used to calculate the activation energy (E_a^*) and some thermodynamic activation functions. The results can be used to understand how inhibition works. By examining the thermodynamic characteristics for MSL dissolution in different acids studied without and in the presence of various molarities of Cys., this work advances our understanding of the adsorption mechanism. The following thermodynamic functions were obtained by using the Arrhenius (eq 16) and transition state (eq 17)[51]

$$\log k = \log A - \left(\frac{E_a^*}{2.303RT}\right) \tag{16}$$

Because it is correlated with the quantity of active centers, the constant A is sometimes referred to as the pre-exponential agent in the context of heterogeneous chemical reactions, T is the Kelvin temperature, and R is the universal gas constant in joules.

$$k = \left(\frac{RT}{Nh}\right)\exp\left(\frac{\Delta S^*}{R}\right)\exp\left(\frac{-\Delta H^*}{RT}\right) \tag{17}$$

where h and N are Planck's constant and Avogadro's number, respectively, and ΔS^* and ΔH^* are the apparent entropy of activation and enthalpy of activation. The Arrhenius and transition state curves were built using chemical measures for MSL in different acids studied (1.0 M) solutions containing various molarities of the Cys. compound in the temperature from 25 to 55 °C. Figures 5 and 6 display the Arrhenius and transition-state graphs of the MSL in different acids (1 M) solutions without and with various molarities from Cys, respectively. The values of the thermodynamic activation functions computed from these curves as a function of Cys. concentration are displayed in Table 1. E_a^*, which is higher in the presence of Cys. molecules than it is in the uncontrolled different acids studied (1.0 M), indicating strong adsorption of the inhibitor particles on the metal surface.[52] Table 1 further

https://doi.org/10.1021/acsomega.3c10522
ACS Omega 2024, 9, 13391−13411

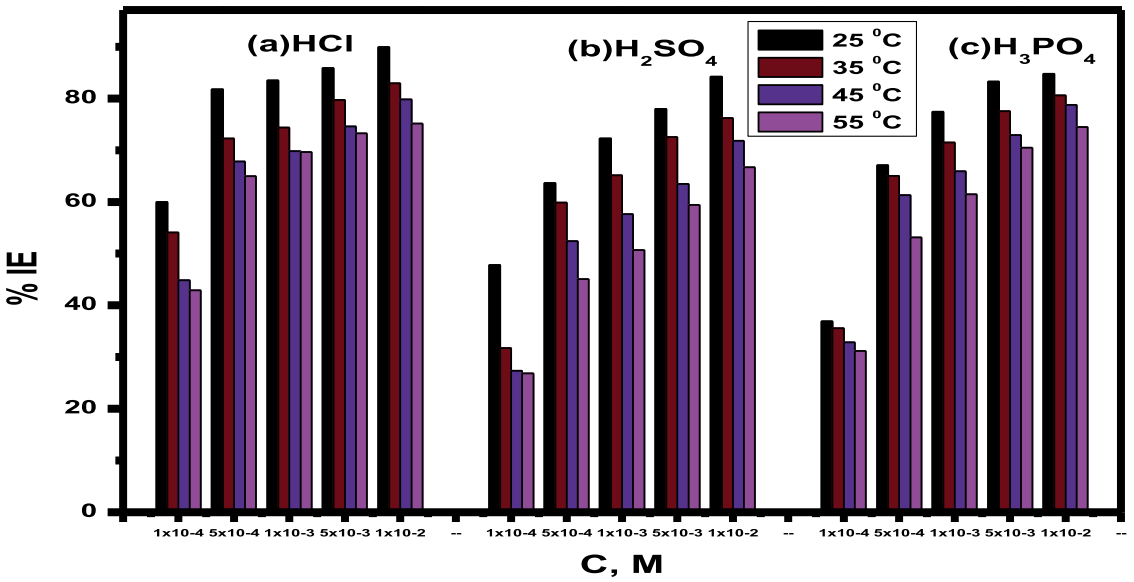

Figure 4. Effect of concentration of Cys. on corrosion inhibition performance (% IE) of MSL in a 1 M solution of: (a) HCl, (b) H_2SO_4, and (c) H_3PO_4 at different temperatures.

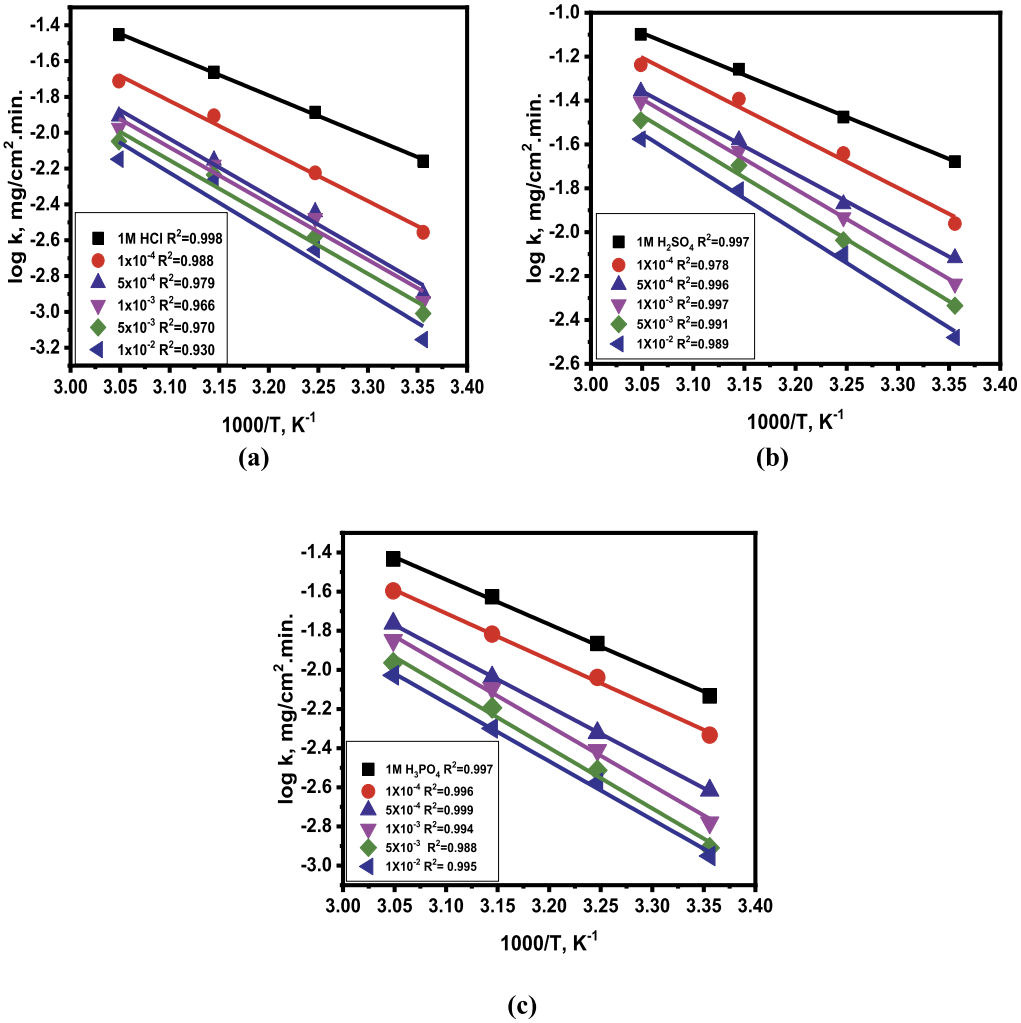

Figure 5. log k vs $1/T$ plots for MSL in a 1 M solution of (a) HCl, (b) H_2SO_4, and (c) H_3PO_4 without and with different concentrations of Cys.

shows that the values of ΔH^* have positive indications, indicating endothermically induced adsorptive attachment of Cys. molecules to the surface of MSL. The presence of Cys. causes an increase in ΔH^*, which denotes an increase in the

https://doi.org/10.1021/acsomega.3c10522
ACS Omega 2024, 9, 13391−13411

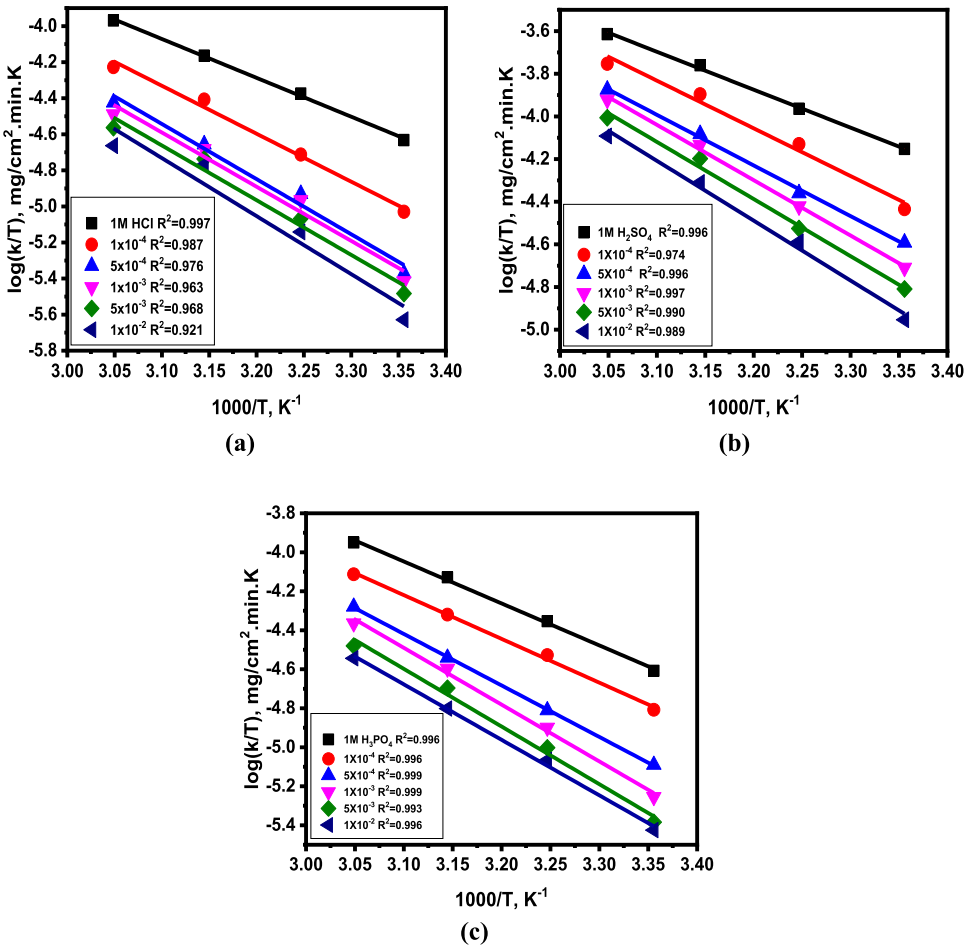

Figure 6. log k/T vs $1000/T$ plots for MSL in a 1 M solution of (a) HCl, (b) H_2SO_4, and (c) H_3PO_4 without and with different concentrations of Cys.

Table 1. Thermodynamic Parameters for MSL in a 1 M Solution of HCl, H_2SO_4 and H_3PO_4 in the Absence and Presence of Different Concentrations of Cys

medium	HCl			H_2SO_4			H_3PO_4		
Conc, M	E_a^*, (kJ mol^{-1})	ΔH^*, (kJ mol^{-1})	ΔS^*, (J mol^{-1} K^{-1})	E_a^*, (kJ mol^{-1})	ΔH^*, (kJ mol^{-1})	ΔS^*, (J mol^{-1} K^{-1})	E_a^*, (kJ mol^{-1})	ΔH^*, (kJ mol^{-1})	ΔS^*, (J mol^{-1} K^{-1})
blank	42.8	40.1	−152.2	36.0	33.4	−166.4	42.4	39.8	−152.8
1×10^{-4}	53.7	51.0	−123.3	44.5	41.9	−142.6	45.7	43.1	−145.4
5×10^{-4}	57.2	54.5	−116.2	47.5	44.9	−136.2	54.5	51.8	−121.8
1×10^{-3}	59.0	56.4	−111.2	52.2	49.6	−122.4	59.2	56.5	−108.3
5×10^{-3}	61.0	58.4	−106.4	54.1	51.5	−118.1	59.6	57.0	−108.9
1×10^{-2}	61.9	59.2	−104.5	55.8	53.2	−114.5	59.7	57.1	−110.1

energy barrier for the corrosion reaction. About 2.6 kJ mol^{-1} is the resultant mean difference between E_a^* and ΔH^*, which is close to the RT value (2.63 kJ mol^{-1}).[53,54] This establishes the unimolecular nature of the reaction that dissolves MSL in 1 M solutions of HCl, H_2SO_4, and H_3PO_4. The values of ΔS^* shown in Table 1 demonstrate that an association rather than a dissociation is signaled by the activated complex during the rate-determining stage, indicating that the disorder occurs along the pathway from reactant to activated complex.[55] Interestingly, Table 1 shows that the activation energy and other parameters in the presence of Cys. in HCl are greater than those in H_2SO_4 and H_3PO_4. This may be due to the fact that the inhibitor molecules are strongly and abundantly absorbed on the surface of the electrode in the presence of hydrochloric acid compared to other acids. This, in turn, may be because chloride ions are easier to absorb to the surface than sulfate and phosphate ions.[56]

3.1.2. Adsorption Study. Cys contains heteroatoms (O, S, and N) which facilitate its adsorption on the MSL surface to form corrosion protective layers.[57] This can be achieved through one or more of the following adsorption possibilities: electrostatic forces between protonated Cys. molecules and the charged MSL surface (physical adsorption), creation of coordination bonds between the unoccupied d-orbital of the substrate and the lone electron pair of heteroatoms (chemisorption), or a combination of both.[43] For this purpose, several adsorption isotherms (Flory−Huggins, Langmuir, Frumkin, Temkin, Freundlich type, and Kinetic model) were studied (see Figures S13−S30). The results indicated that the adsorption of Cys on the MSL surface follows the Langmuir isotherm as shown by the

https://doi.org/10.1021/acsomega.3c10522
ACS Omega 2024, 9, 13391−13411

Table 2. Adsorption Parameters of Langmuir Isotherm for Corrosion of MSL in Molar Solutions of Different Acids in the Existence of Cys. (1×10^{-2}) at Different Temperatures (Obtained from WL Experiments)

temp °C	R^2	log K_{ads} M^{-1}	$-\Delta G_{ads}$ (kJ mol^{-1})	$-\Delta H_{ads}$ (kJ mol^{-1})	ΔS_{ads} (J mol^{-1} K^{-1})
			HCl		
25	0.999	3.95	32.49	25.37	23.89
35	0.999	3.90	33.29		25.71
45	0.999	3.72	33.27		24.84
55	0.998	3.56	33.31		24.20
			H_2SO_4		
25	0.998	3.67	30.90	21.22	32.48
35	0.999	3.56	31.28		32.66
45	0.995	3.42	31.44		32.14
55	0.996	3.34	31.93		32.65
			H_3PO_4		
25	0.999	3.82	31.75	17.99	46.17
35	0.999	3.72	32.22		46.20
45	0.998	3.60	32.54		45.75
55	0.999	3.54	33.19		46.34

regression correlation coefficient (R^2) values listed in Table 2, derived from the following equation[58,59]

$$\frac{C_{inh}}{\theta} = \frac{1}{K_{ads}} + C_{inh} \quad (18)$$

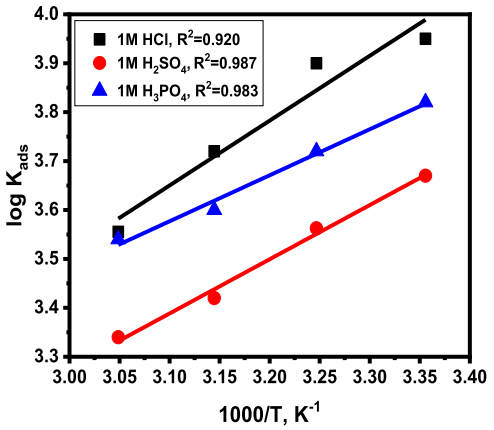

Figure 8. log K_{ads} vs $1/T$ for corrosion of MSL in a 1 M solution of HCl, H_2SO_4 and H_3PO_4 in the presence of Cys(1×10^{-2}).

where (θ) is calculated using the WL method, K_{ads} is the adsorption−desorption equilibrium constant for the metal substrate processes, and C_{inh} is the molarity of the studied Cys. inhibitor. On the chart of C compared to C/θ, a straight line with a slope and correlation coefficient close to one can be seen (Figure 7). To get the common free energy of adsorption (ΔG_{ads}) from (K_{ads}), the following formula was used[60]

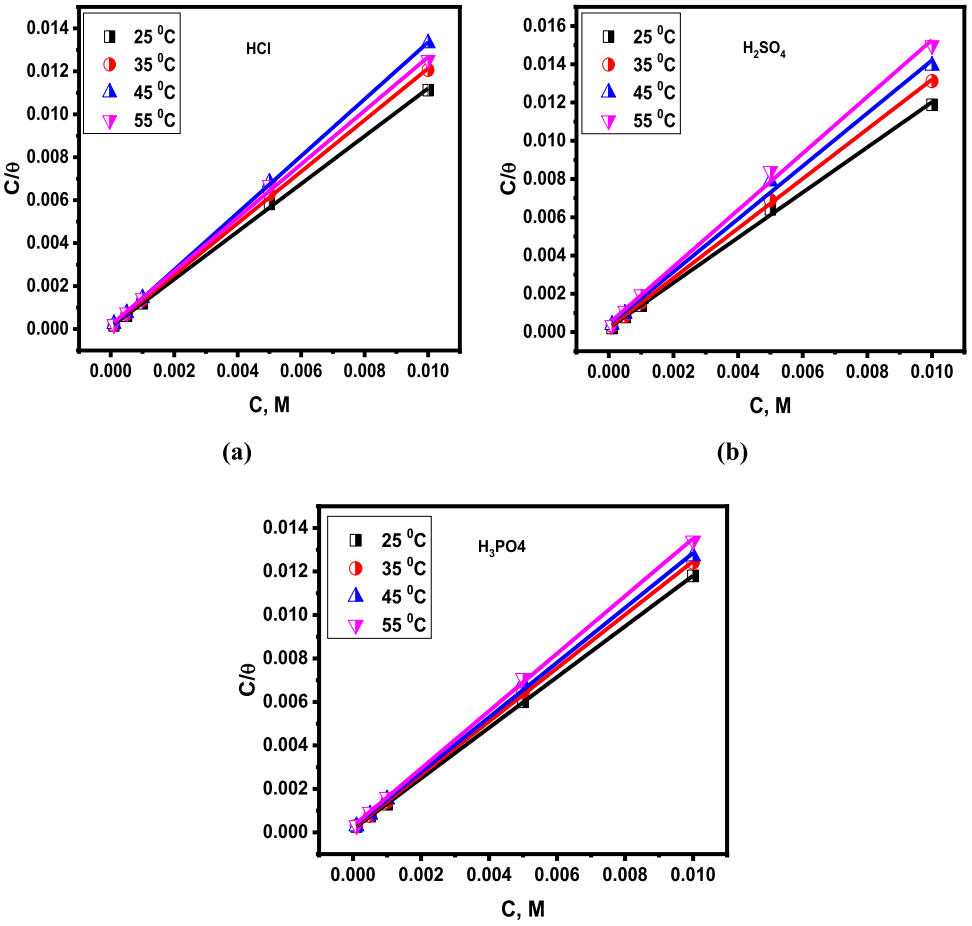

Figure 7. Plots of C/θ vs C of Cys. for corrosion of MSL in a 1 M solution of (a) HCl, (b) H_2SO_4 and (c) H_3PO_4 at different temperatures (data obtained from WL experiments).

https://doi.org/10.1021/acsomega.3c10522
ACS Omega 2024, 9, 13391−13411

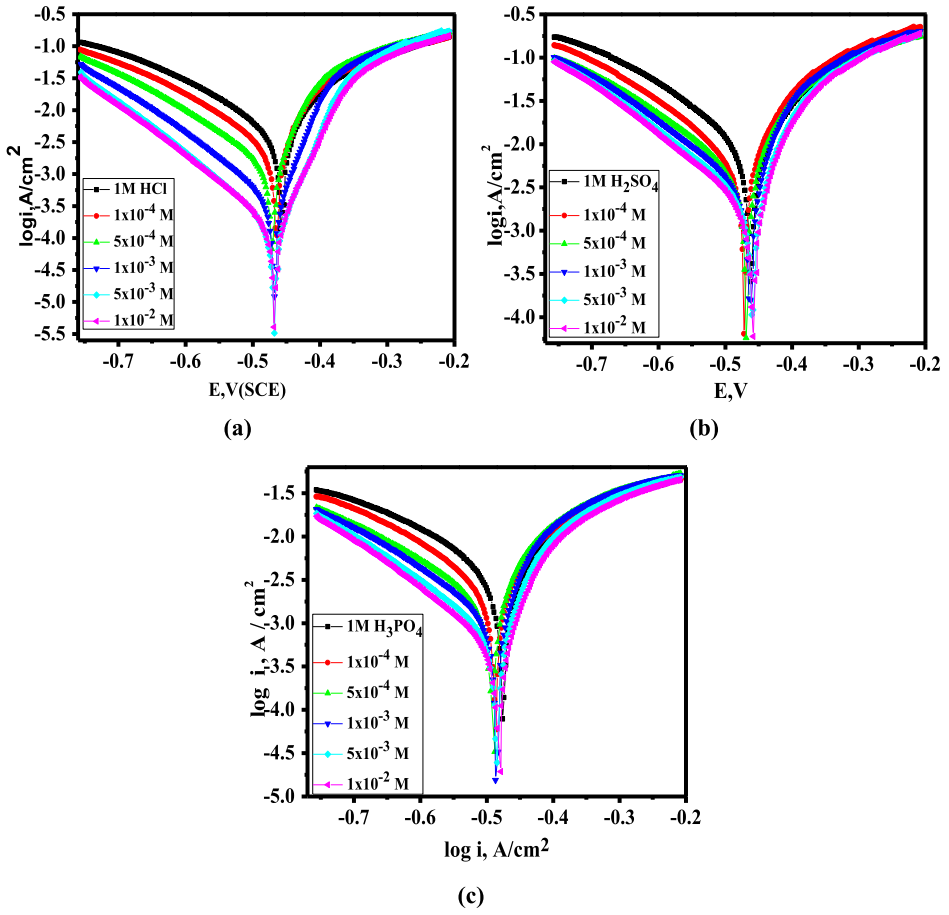

Figure 9. PDP curves for corrosion of MSL in a 1 M solution of: (a) HCl, (b) H_2SO_4 and (c) H_3PO_4 at different temperatures without and with different concentrations of Cys.

Table 3. Effect of Concentration of Cys. on the Electrochemical Parameters Calculated by Using PDP for the Corrosion of MSL in a 1 M Solution of HCl, H_2SO_4 and H_3PO_4

Conc. M	$-E_{corr}$, mV	i_{corr}, (μA cm^{-2})	$-\beta_c$, (mV dec^{-1})	β_a, (mV dec^{-1})	R_p (Ω cm)	C.R mm/yr	θ	% IE
				HCl				
blank	457.5 ± 5	8617 ± 23	258.9 ± 5	185.5 ± 2	5.446 ± 0.6	100.0 ± 3		
1×10^{-4}	465.2 ± 6	5513 ± 18	245.7 ± 4	163.1 ± 3	7.720 ± 0.5	64.00 ± 2	0.360	36.0
5×10^{-4}	471.4 ± 4	2732 ± 17	211.2 ± 3	170.8 ± 2	12.84 ± 0.4	31.72 ± 0.9	0.683	68.3
1×10^{-3}	468.1 ± 3	614.0 ± 15	250.5 ± 5	196.1 ± 3	41.49 ± 0.5	7.127 ± 0.5	0.929	92.9
5×10^{-3}	468.0 ± 4	239.1 ± 9	239.9 ± 3	184.9 ± 4	95.93 ± 0.7	2.776 ± 0.2	0.972	97.2
1×10^{-2}	468.3 ± 2	228.9 ± 7	232.1 ± 2	182.2 ± 5	96.16 ± 30.8	2.657 ± 0.2	0.973	97.3
				H_2SO_4				
blank	461.6 ± 4	19400 ± 26	300.5 ± 4	221.4 ± 3	2.854 ± 0.1	225.22 ± 5		
1×10^{-4}	471.7 ± 3	12620 ± 21	277.5 ± 3	235.0 ± 2	3.820 ± 0.2	146.51 ± 3	0.349	34.9
5×10^{-4}	469.0 ± 5	8995 ± 24	283.6 ± 3	237.1 ± 3	5.264 ± 0.3	104.41 ± 4	0.536	53.6
1×10^{-3}	462.9 ± 2	5539 ± 22	278.9 ± 4	242.9 ± 4	7.012 ± 0.4	64.29 ± 2	0.714	71.4
5×10^{-3}	459.7 ± 6	4033 ± 21	258.6 ± 2	233.7 ± 3	9.082 ± 0.2	26.82 ± 0.5	0.792	79.2
1×10^{-2}	458.8 ± 3	3031 ± 19	262.3 ± 5	224.8 ± 5	10.90 ± 0.3	16.35 ± 0.6	0.844	84.4
				H_3PO_4				
blank	475.3 ± 6	9984 ± 27	412.0 ± 4	358.7 ± 5	9.175 ± 0.2	115.89 ± 2		
1×10^{-4}	486.8 ± 7	7258 ± 25	390.0 ± 5	304.2 ± 4	11.05 ± 0.3	84.25 ± 1	0.273	27.3
5×10^{-4}	491.5 ± 8	3715 ± 15	371.3 ± 3	376.9 ± 6	19.38 ± 0.5	43.09 ± 0.7	0.628	62.8
1×10^{-3}	485.9 ± 5	1955 ± 16	373.6 ± 5	370.6 ± 3	23.34 ± 0.6	22.70 ± 0.5	0.804	80.4
5×10^{-3}	485.3 ± 7	1684 ± 13	397.8 ± 6	366.1 ± 5	27.50 ± 0.7	19.55 ± 0.8	0.831	83.1
1×10^{-2}	482.3 ± 6	1028 ± 11	394.7 ± 4	346.7 ± 4	38.76 ± 0.4	11.93 ± 0.9	0.897	89.7

$$K_{ads} = \frac{1}{55.5}\exp\frac{-\Delta G^{\circ}_{ads}}{RT} \quad (19)$$

At the solution/metal interface, the water concentration is 55.5 (mol/L), and R stands for the gaseous universal constant (8.314 J/mol). The adsorption strength of Cys. molecules on MSL

https://doi.org/10.1021/acsomega.3c10522
ACS Omega 2024, 9, 13391−13411

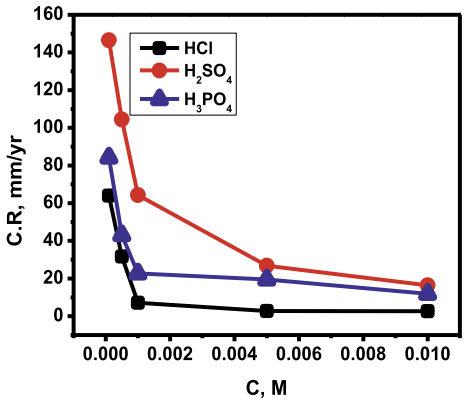

Figure 10. Comparison of C.R of MSL in three different acids in the presence of varying concentrations of cysteine. The data points obtained from PDP.

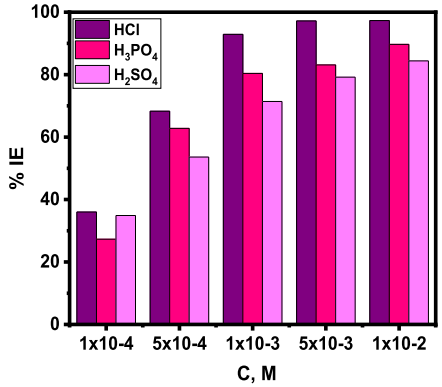

Figure 11. Plots of % IE vs concentration of Cys. for corrosion of MSL in a 1 M solution of HCl, H_2SO_4, and H_3PO_4. The data points obtained from PDP.

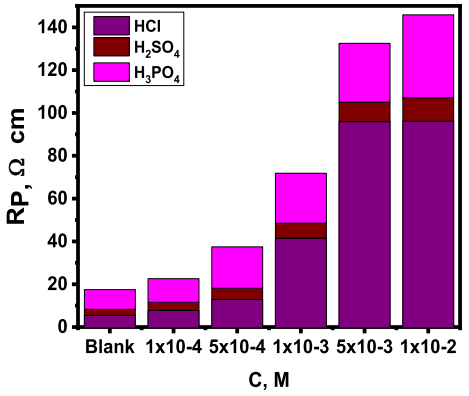

Figure 12. Plots of R_P against different concentrations of Cys. for MSL in a 1 M solution of HCl, H_2SO_4, and H_3PO_4. The data points obtained from PDP.

represents by K_{ads}. A greater K_{ads} value, for instance, shows that the Cys. molecules are more tightly bonded to the MSL's surface. The Vant Hoff equation was used to calculate the enthalpy of adsorption (ΔH°_{ads}) as follows[61]

$$\log K_{ads} = \frac{-\Delta H^{\circ}_{ads}}{2.303RT} + \text{constant} \quad (20)$$

For MSL in 1 M HCl, 1 M H_2SO_4, and 1 M H_3PO_4, Figure 8 shows the log K_{ads} against $1/T$ plotted. The formula used for calculating the entropy of adsorption (ΔS°_{ads}) was as follow

$$\Delta S^{\circ}_{ads} = \frac{\Delta H^{\circ}_{ads} - \Delta G^{\circ}_{ads}}{T} \quad (21)$$

For MSL in various acid solutions at various temperatures, the values of K_{ads}, ΔG°_{ads}, ΔH°_{ads}, and ΔS°_{ads} were listed in Table 2 according to Langmuir adsorption isotherms. The inverse of ΔG°_{ads}, with a negative sign, indicates the spontaneity of the adsorption process.[62] Physical adsorption is created when charged (protonated) Cys. molecules contact electrostatically with a negatively charged MSL surface. In terms of preventing corrosion, chemisorption and physisorption are the two adsorption types that are commonly taken into consideration. Among −20 and −40 kJ mol^{-1}, when the reading heads are set to −40 kJ mol^{-1}, chemical adsorption typically wins out over physical adsorption; however, at −40 kJ mol^{-1}, only chemical adsorption happens. Readings up to −20 kJ mol^{-1} from ΔG^{0}_{ads} are regular with physical adsorption. The higher ΔG^{0}_{ads} values in Table 2 show that the mechanism of adsorption of Cys. on the surface of MSL in 1 M solutions of HCl, H_2SO_4, and H_3PO_4, includes both electrostatic adsorption and chemical adsorption but the generated compound largely exhibits chemical adsorption, which is brought on by the transfer of electrons from high electron centers to iron's open 3d orbital, forming a covalent bond.[63] The exothermal adsorption of Cys. on MSL in 1 M solutions of HCl, H_2SO_4, and H_3PO_4 is indicated by the negative sign of ΔH°_{ads}. According to the calculated ΔS°_{ads} values, the entropy decreases during the adsorption process.

3.2. Potentiodynamic Polarization. Figure 9a−c demonstrates the PDP curves for MSL corrosion in various acidic corrosive environments without and with Cys. The intersection of the anodic and cathodic Tafel lines of the polarization curves was used to determine the corrosion potential (E_{corr}), i_{corr}, anodic and cathodic Tafel slopes (βa and βc), and polarization resistance (R_p). Table 3 contains a list of all the obtained potentiodynamic parameters. It is evident from the PDP curves that in all of the corrosive media examined, the anodic and cathodic curves with Cys. were pushed toward the direction of decreased current density when compared to the blank. This result suggested that Cys. might inhibit the cathodic and anodic reactions.[64] The βa and βc slopes did not alter considerably with a rise in Cys. concentration, indicating that the inhibitory mechanism has not changed.[65] Also, due to the low volatility in the acquired E_{corr} values, E_{corr} statistics demonstrate that the Cys. compound under research exhibit mixed-type inhibitor behavior.[66]

Figure 10a,b shows a comparison of the corrosion rate of MSL in 1 M HCl, H_2SO_4, and H_3PO_4 using data from PDP measurements without and with different concentrations of Cys. It is observed that in the absence of Cys. the CR of MSL in H_2SO_4 is higher than that in H_3PO_4 and HCl (i.e., H_2SO_4 > H_3PO_4 > HCl). Figure 11 displays a plot of % IE against Cys. concentration for MSL corrosion in 1 M solution of HCl, H_2SO_4, and H_3PO_4 as determined by PDP. It can be seen that % IE increases with increasing Cys concentration, in contrast to the rise in C.R. in different acidic solutions, where % IE in HCl rises greater than % IE in H_3PO_4 and % IE in H_2SO_4 (i.e., HCl > H_3PO_4 > H_2SO_4). Increasing the Cys concentration leads to improved polarization resistance due to the adsorption of the inhibitor molecules on the MSL surface, as shown in Figure 12.[67]

https://doi.org/10.1021/acsomega.3c10522
ACS Omega 2024, 9, 13391−13411

Table 4. Electrochemical Kinetic Parameters Extracted From EIS Technique for the Corrosion of MSL in a 1 M Solution of HCl, H_2SO_4, and H_3PO_4 at Different Concentrations of Cys

medium	Conc., M	R_{ct}, (Ω cm^2)	R_s, (Ω cm^2)	Y_0, μS^n/Ω cm^2	n	C_{dl}, (μF cm^{-2})	θ	% IE
HCl	blank	17.17 ± 0.43	0.4738 ± 0.0032	418.6 ± 7.3	912 ± 4.6	260.77		
	1×10^{-4}	45.17 ± 1.02	0.4193 ± 0.0043	241.7 ± 4.7	914 ± 4.2	158.01	0.620	62.0
	5×10^{-4}	89.51 ± 2.10	0.5381 ± 0.0043	226.2 ± 4.3	897 ± 3.9	144.27	0.808	80.8
	1×10^{-3}	109.7 ± 2.17	0.4794 ± 0.0039	227.6 ± 3.8	901 ± 4.1	151.94	0.843	84.3
	5×10^{-3}	164.4 ± 2.10	0.4889 ± 0.0040	337.5 ± 5.8	881 ± 3.7	228.12	0.896	89.6
	1×10^{-2}	188.5 ± 2.30	0.4929 ± 0.0039	250.1 ± 4.9	892 ± 4.5	166.52	0.908	90.8
H_2SO_4	blank	1.325 ± 0.036	0.5535 ± 0.0021	805.0 ± 8.5	929 ± 3.6	477.15		
	1×10^{-4}	1.716 ± 0.037	0.5183 ± 0.0011	485.0 ± 6.4	926 ± 2.9	275.41	0.228	22.8
	5×10^{-4}	3.416 ± 0.029	0.5670 ± 0.0031	436.4 ± 5.7	911 ± 3.4	231.07	0.612	61.2
	1×10^{-3}	4.779 ± 0.033	0.6081 ± 0.0029	397.2 ± 4.2	905 ± 2.8	211.14	0.723	72.3
	5×10^{-3}	7.630 ± 0.031	0.5923 ± 0.0025	380.3 ± 3.6	907 ± 3.1	209.50	0.826	82.6
	1×10^{-2}	8.715 ± 0.023	0.5904 ± 0.0024	361.2 ± 3.7	894 ± 2.7	177.41	0.847	84.7
H_3PO_4	blank	3.564 ± 0.017	0.3857 ± 0.0014	452.3 ± 5.6	875 ± 2.5	180.95		
	1×10^{-4}	6.865 ± 0.070	0.3521 ± 0.0017	359.8 ± 5.2	865 ± 4.2	141.31	0.481	48.1
	5×10^{-4}	10.37 ± 0.040	0.3149 ± 0.0023	397.5 ± 4.4	845 ± 3.9	145.61	0.656	65.6
	1×10^{-3}	14.78 ± 0.030	0.3884 ± 0.0034	338.6 ± 3.9	856 ± 4.1	139.29	0.759	75.9
	5×10^{-3}	29.05 ± 0.020	0.4256 ± 0.0028	306.5 ± 3.1	877 ± 3.8	158.17	0.877	87.7
	1×10^{-2}	31.91 ± 0.050	0.3671 ± 0.0029	310.1 ± 2.8	863 ± 3.6	140.68	0.887	88.7

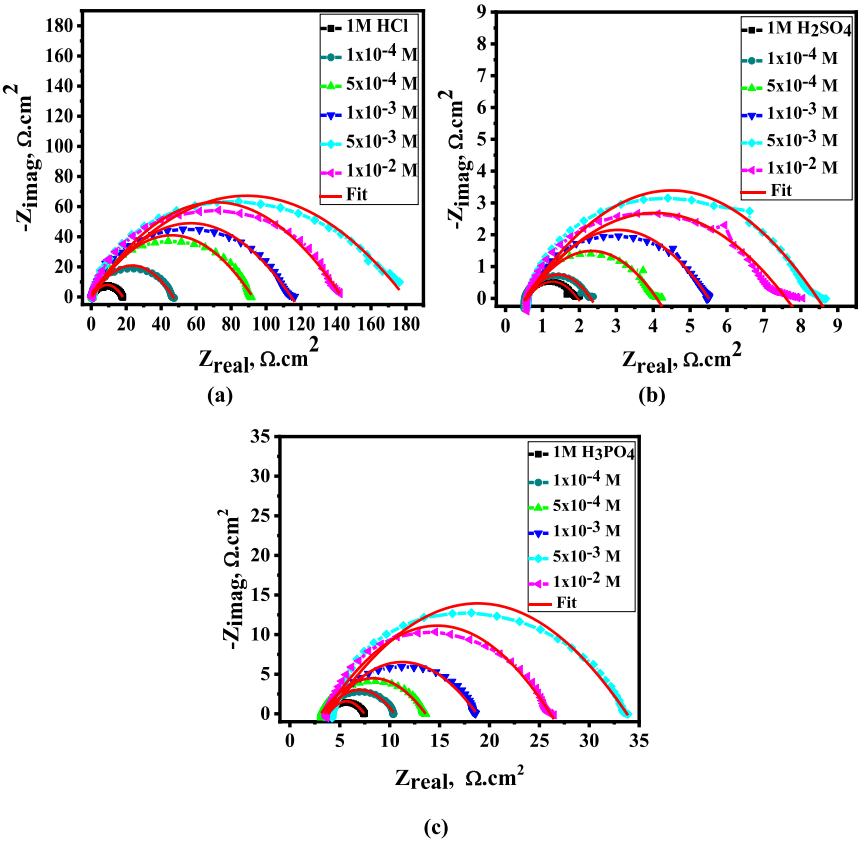

Figure 13. Nyquist plots for corrosion of MSL in a 1 M solution of: (a) HCl, (b) H_2SO_4, and (c) H_3PO_4 without and with different concentrations of Cys.

3.3. Electrochemical Impedance Spectroscopy. In the corrosion papers,[68−71] the EIS approach is a thorough inspection. There are two lines and two ions in the complex environment that surrounds the MSL/electrolyte contact, one of which is positively charged and the other is negatively charged. Hence, a variety of impedances are produced in the oxide layer that covers the alloy electrode's surface as a result of the ions that diffuse into the MSL surface and the charges that move in and out of it. Moreover, the electrical double layer (C_{dl}), resistance of charge transfer (R_{ct}), and resistance of solution (R_s) are all present in the oxide coating. A summary of the EIS measurements made on MSL electrodes submerged in different acid solutions containing various concentrations of Cys. corrosion inhibitor at 25 °C is shown in Table 4. The Nyquist and Bode graphs of MSL in different acid solutions containing various concentrations of Cys. are shown in Figures 13a−c and

https://doi.org/10.1021/acsomega.3c10522
ACS Omega 2024, 9, 13391−13411

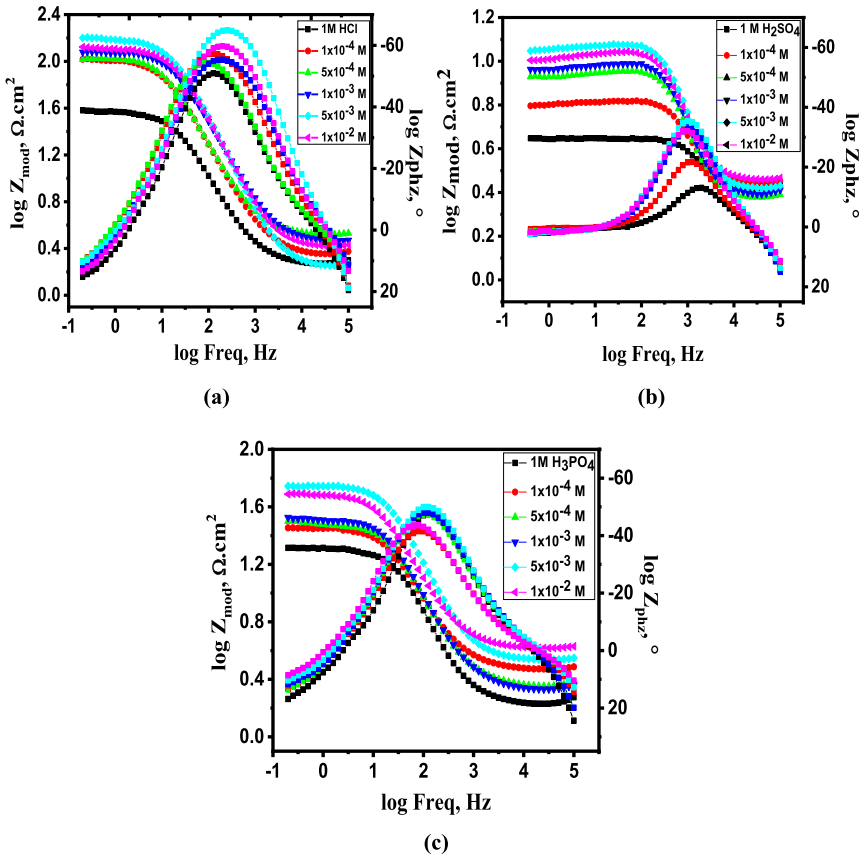

Figure 14. Bode plots for corrosion of MSL in a 1 M solution of: (a) HCl, (b) H_2SO_4, and (c) H_3PO_4 without and with different concentrations of Cys.

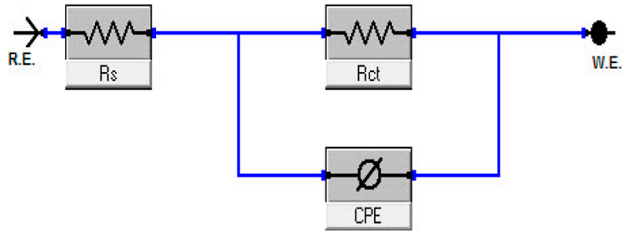

Figure 15. EC used in EIS data fitting.

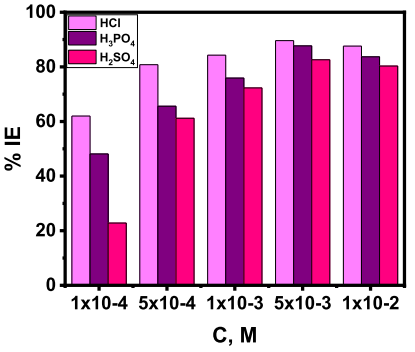

Figure 16. Plots of % IE against concentration of Cys. for corrosion of MSL in a 1 M solution of HCl, H_2SO_4, and H_3PO_4 as obtained from EIS.

14a−c, respectively. In order to examine the impedance data, an EC similar to the one in Figure 15 was used. In order to account for several forms of nonhomogeneities typical of corroding electrodes, such as surface roughness, inadequate polishing, grain boundaries, and surface contaminants, R_s is the solution resistance and constant phase elements (CPE) are used in place of capacitors.[72−75] In the Nyquist diagram, increased Cys. concentration throughout the corrosion process causes the semicircle's diameter to increase as a result of higher charge-transfer resistance.[76] In order to increase corrosion resistance and decrease corrosion rate, the selected corrosion inhibitor are adsorbed at the electrolyte/metal contact. When different amounts of the Cys. substance are added, the local dielectric constant decreases and/or the electrical double layer rises, which results in a reduction in the double layer's capacitance in comparison to the control solution. Cys. adsorption molecules are found in the MSL interface or solution as a result.[77−79] Nyquist plots were not close as predicted and revealed a departure from EIS theory. Due to frequency dispersion and the variability of the MSL surface, semicircle mismatch is observed instead of the perfect condition.[80] Figure 14a−c shows the impedance measurements made for the MSL electrode using Bode diagrams of impedance size (|Z|) and full-frequency angle of phase at various inhibitor doses. For large quantities of Cys., phase angles and impedance at low frequencies increase, indicating better protective function.[81] Its parallel adsorption on the MSL/solution interface is likely what causes the Cys. compound's inhibiting effects. An active center with one or more adsorbers is what causes parallel adsorption. The process of chemical adsorption involves the metal and the adsorbed molecules of the Cys. compound forming a chemical connection. Charge transfer from the inhibitor molecule to the MSL surface creates a coordinated sort of connection during chemical adsorption.[82−84] Given that the impedance of MSL depends on the frequency, we used the parameters (n and Y_0) in

https://doi.org/10.1021/acsomega.3c10522
ACS Omega 2024, 9, 13391−13411

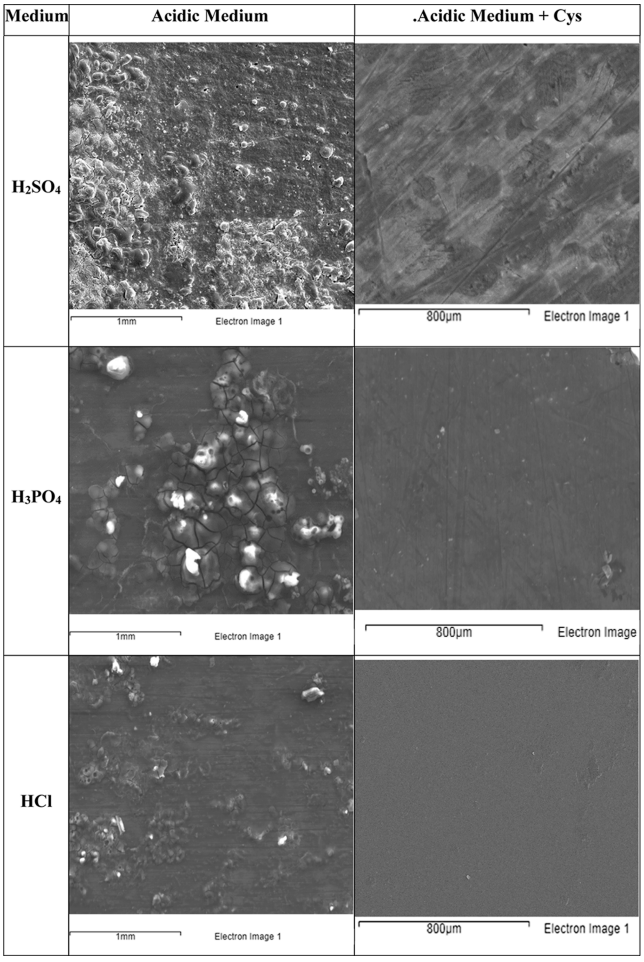

Figure 17. SEM micrographs of MSL surface after exposure to a 1 M solution of HCl, H_2SO_4, and H_3PO_4 for 24 h in the absence and presence of 1×10^{-2} M of Cys.

our test to provide a mathematical expression for the frequency.[85]

$$Z_{CPE} = Y_0^{-1}(J\omega)^{n-1} \quad (22)$$

For the letters $j^2 = -1$ is the imaginary number, $\omega = 2\pi f$ is the sinewave's angular frequency, where f is the frequency of AC, and Y_0 is CPE coefficient. Because of several factors, including electrode roughness, the dielectric constant, and surface heterogeneity, the range of n values in actual experimental settings is 0 to 1. When compared to the inhibition system, the n value of various acid solutions is high in our investigation. As the Cys. concentration rises, the rate decreases, showing that the inhibitor adsorption is not uniform but that the MSL's surface is relatively homogeneous.[86]

Figure 16 shows plotting % IE against concentration of Cys. for corrosion of MSL in 1 M HCl, 1 M H_2SO_4, and 1 M H_3PO_4 as obtained from EIS. As shown from this Figure, % IE increases with increasing Cys. concentration in all the used corrosive mediums, but % IE in HCl > % IE in H_3PO_4 > % IE in H_2SO_4. The order of % IE in the acidic solutions using EIS technique is in agreement with that obtained using WL and PDP techniques.

3.4. Scanning Electron Microscopy. The SEM images of the MSL surface following exposure to 1 M HCl, 1 M H_2SO_4, and 1 M H_3PO_4 solutions for 24 h in the absence and presence of the optimum concentration (1×10^{-2} M) of the examined inhibitor (Cys.) are shown in Figure 17. These micrographs clearly show that the MSL surface exposed to the acidic solutions devoid of Cys. is rough and porous, and thick coatings of corrosion products were found as a result of the steel dissolving in the abrasive solutions. The biggest amount of MSL was dissolved by the H_2SO_4 solution, then the H_3PO_4 solution, and the least amount was by the HCl solution. Also, a smooth MSL surface showed considerable corrosion resistance when utilizing the studied Cys. inhibitor in the acidic conditions. In contrast to Cys. in H_3PO_4 and H_2SO_4, the steel surface was smoother when Cys. was present in HCl. The results show that Cys. in HCl effectively controls the harmful attack of HCl solution, and they also demonstrate the production of a protective film on the surface of MSL, which increases the effectiveness of inhibition. These outcomes match the electrochemical outcomes quite closely.

3.5. Theoretical Studies. *3.5.1. Computed Quantum Chemistry.* Following the Dmol3 computations for Cys. molecules, snapshots for the optimized structures, HOMO, and LUMO were captured and assembled in Figure 18. Frontier molecular orbitals theory, which were used to describe how reactively the two molecules were (FMO). The ability of molecules to transfer electrons into open molecular orbitals of the proper acceptor is measured by E_{HOMO}. The likelihood of a molecule to accept electrons from another is instead estimated by E_{LUMO}. The greater the molecule's capacity to accept electrons, the lower is its E_{LUMO} value.[87] Therefore, the more electrons that a molecule can donate to the empty d-orbital of metallic iron at the surface, the higher its E_{HOMO} value, and as a result, the more inhibitory power it will be able to exert. Table 5's findings demonstrate that the Cys. molecule has a high energy E_{HOMO}. Thus, it will have the strongest corrosion prevention effect.[88,89] The size of the energy gap (ΔE), which controls whether or not Cys. molecules are reactive during adsorption on the MSL surface, is another crucial factor. The reaction that occurs during adsorption and the magnitude of ΔE are inversely correlated. Low energy gap compounds are effective corrosion inhibitors because it only requires a small amount of ionization energy to dislodge an electron from its outer shell orbit.[90] Table 5 shows that the Cys. has a smaller energy gap (ΔE) in the Neutral form compared to the protonated form, which would mean that the Cys. reacts to the surface of MSL more potently in the Neutral form.[91] Softer molecules are produced by smaller energy gaps than by bigger ones. Soft molecules respond more quickly than harder molecules because they have a faster electron transport time to their acceptor. The composition, constancy, and reactivity of molecules can be ascertained using the absolute hardness (η) and softness (σ) values. The molecules of the Cys. change into Lewis bases, whereas the MSL transforms into a Lewis acid in the corrosion structure. For avoiding acid corrosion in bulk metals that take mild acids into consideration, soft-base inhibitors are the most effective. The construction is moved and rationalized using the dipole moment, which is the third critical parameter.[92,93] The chance that stronger interactions between the Cys. molecules and the MSL surface were made, leading in a greater % IE and better adsorption, is taken into account when comparing data. The physical adsorption of the Cys. onto the MSL surface is accelerated by the electrostatic attraction between an organic dipole and an excited MSL surface. Consequently, the higher dipole moment of the adsorption molecules is preferable. By measuring the dipole moments, it was found that the form of the dipole torque significantly different in protons, indicating that the Cys. is physically adsorbed on the MSL surface as a proton

https://doi.org/10.1021/acsomega.3c10522
ACS Omega 2024, 9, 13391−13411

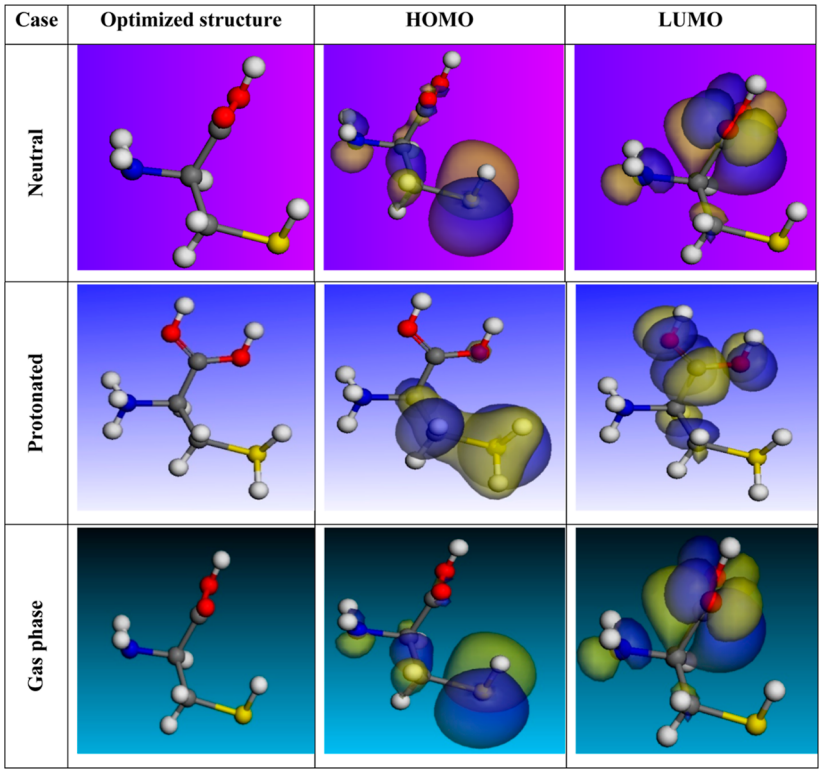

Figure 18. Molecular structure optimization and geometry of the HOMO and LUMO orbitals for Cys. in neutral, protonated, and gas phase using the Dmol3/GGA/BOP methodology.

Table 5. Quantum Data for Cys. in Neutral, Protonated, and Gas Phase

parameters	neutral	protonated	gas
$-E_{HOMO}$ (eV)	−5.671	−10.080	−5.980
$-E_{LUMO}$ (eV)	−1.314	−4.071	−1.652
ΔE (eV)	4.35	6.01	4.33
η (eV)	2.18	3.00	2.17
σ (eV)$^{-1}$	0.458	0.33	0.460
μ (e.V)	−3.49	−7.07	−3.82
χ(eV)	3.49	7.07	3.82
dipole moment (debyes)	2.5002	2.0075	1.9662
molecular area (Å^2)	146.587646	150.329568	
ω(electrophilicty index)	2.79	8.33	3.36
ω^+ (electro-accepting power)	1.33	5.169	1.727
ω^- (electro-donating)	4.818	14.68	5.54
ε(nucleophilicity index)	0.358	0.120	0.297
ΔE back-donation	−0.545	−0.75	−0.543
ΔN_{max} (e)	0.300	−0.378	−0.226

can be.[94] Despite this, there is not any proof in the literature that it influences inhibitory efficacy.[95] If ΔN is smaller than 3.6, it is believed that the metal surface's electronic inhibitor will boost the effectiveness of the inhibition.[96] The ability of an electron to bind Cys. is known as electronegativity (χ). When a MSL surface is more eager to absorb an electron, the value of χ_{inh} rises (a protonated form is more valuable). Inhibition is strengthened as a result of the stronger surface contacts between Cys. particles with higher electronegativity and the surface of MSL. Table 5 demonstrates the Cys. 's potent inhibitory action in comparison to earlier studies.[97−100] By expanding the area where those molecules may interact with the surface of MSL, larger Cys. molecules have a greater inhibitory impact. A useful indicator of

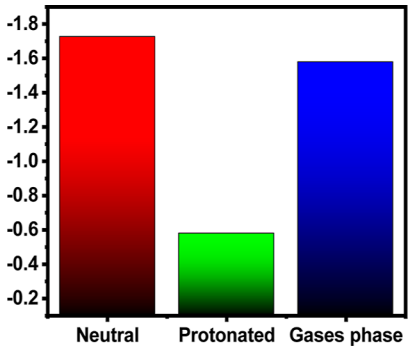

Figure 19. Protonated and nonprotonated Cys. compound using TNC.

electron donation and charge transfer from MSL to Cys. molecules are the positive values of hardness (η) and consequently the negative values of back-donation energy ($\Delta E_{back\text{-}donation} = -\eta/4$).[101] This improves the ability of Cys. to bind to MSL surfaces and preventing corrosion. In terms of the nucleophilicity index (ε), we discovered that Cys. has higher numerical values in its neutral form in gas and liquid phases than Cys. in the protonated form. Hence, Cys. has a significant nucleophilic property in the protonated form. This demonstrates that the Cys. molecule may support electrons on the surface of MSL. Recently, the ability of inhibitors to collect or donate electrical charge was determined using the electron-accepting power $[\omega^+ = (I + 3A)^2/16(I - A)]$ and the electrodonating $[\omega^- = (3I + A)^2/16(I - A)]$, respectively.[102] According to our research, $\omega^- > \omega^+$ for Cys. in all the circumstances. This indicates that the donating power is dominant and exhibits strong binding to the steel surface to prevent corrosion.

https://doi.org/10.1021/acsomega.3c10522
ACS Omega 2024, 9, 13391−13411

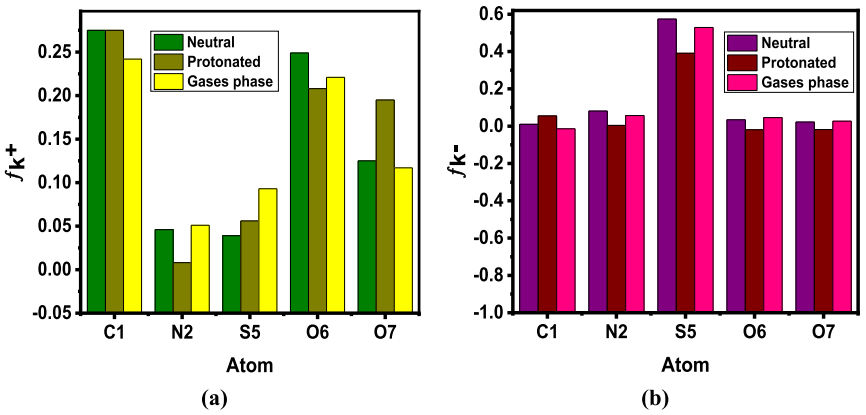

Figure 20. A graphic depiction of Cys.'s Fukui indices for its more reactive atoms in both their protonated (a) and unprotonated (b) forms.

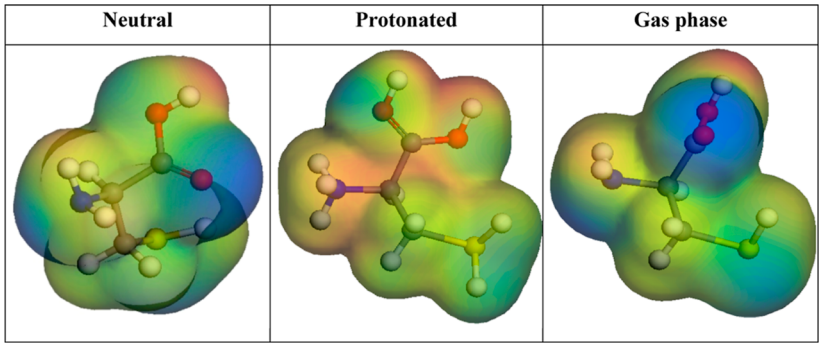

Figure 21. Electrostatic potentials of the Cys. molecules that are protonated and unprotonated, as well as the contour of the inhibitor's electrostatic field.

3.5.1.1. Mulliken Charges and Fukui Indices. Mulliken atomic charges and Fukui indices will be used to determine the location of the donor and acceptor of the molecule's active centers. The fact that the Mulliken distribution values are both negative and positive shows that the donor−acceptor active sites in the Cys. compound increase these species' sensitivity to MSL atoms (Tables S4−S5). The picture in Figure 19 shows similar trend in standings of total negative charge (TNC), with the TNC decreasing as the Cys. was protonated.[103] This demonstrates an increase in the structural interaction of protonated particles through the electrostatic attraction between Cys. protonated constituent and the chloride ion that adsorbed on the surface of the MSL. Organic molecules containing heteroatoms can protonate in these environments, producing positively charged particles, when there is an acidic environment present (HCl). The Cys. molecules interact with the chloride anions, which are widely scattered on the tissue's surface. Here, this idea will be used to study how protonation affects the local centers of Cys. that restrict growth. The atoms of the Cys. compound under study are shown in Figure 20 with increased data of f_k^+ and f_k^- in both protonated and unprotonated systems as additional markers (Fukui's index). The Cys. molecule in this image has specific atoms for both electrophilic and nucleophilic assault systems, according to the examination of the entire Figure. The atom in the Cys. compound that has the maximum Fukui function (f_k^+), is connected to the LUMO, improves reactivity to donor reagent, and is frequently attacked by nucleophiles is also the one that has the highest Fukui function. The target molecule's atom with the uppermost value of the HOMO-related Fukui function (f_k^-), which also provides reactivity in the direction of an acceptor substance, is chosen for electrophilic attack. As a result of protons H+ blocking the cores of the atoms, the values of atoms with a negative charge (f^-) decreased in the protonated state while those with positive charges (f^+) increased since these atoms could now accept electrons (Figure 20). The Cys. compound also contains separate atoms with varying f^+ and f^- values, which implies it can supply and receive electrons in two different circumstances (protonated and neutral organizations).

3.5.1.2. Molecular Electrostatic Potential. The molecular electrostatic potential (MESP) has been used for a long time to pinpoint the location of a chemical reaction. On the surfaces of the electron density, the electrostatic potential has a variety of colors (Figure 21). The red zone, which represents the electrically active and electrophilic zone, is located in a region with a predominantly negative electrostatic potential. Green indicates locations with low probability, whereas blue areas (the nucleophilic zone) have the highest positive electrostatic potential.[104] High electron density regions are where the majority of heteroatoms and double conjugate bonds can be located. Oxygen, sulfur, and nitrogen groups are indicators of electrophilic attack-favorable negative zones.

3.5.2. Monte Carlo Investigation. The ideal structures (adsorbent) in the corrosion-simulating fluid are $250H_2O$ molecules plus $10H_3O^+$ and 10 Cl^- for hydrochloric acid, $250H_2O$ molecules plus $20H_3O^+$ and $10SO_4^{-2}$ for sulfuric acid, and $250H_2O$ molecules plus $30H_3O^+$ and PO_4^{-3} for phosphoric acid were chosen for the adsorption of Cys. (adsorbate) on the Fe(110) crystal. The views of the iron (110) substrate were taken from the top and sideways, respectively. The adsorption processes of neutral and protonated Cys. molecules are shown in Figure 22. Table 6 lists the outcomes of the Monte Carlo

https://doi.org/10.1021/acsomega.3c10522
ACS Omega 2024, 9, 13391−13411

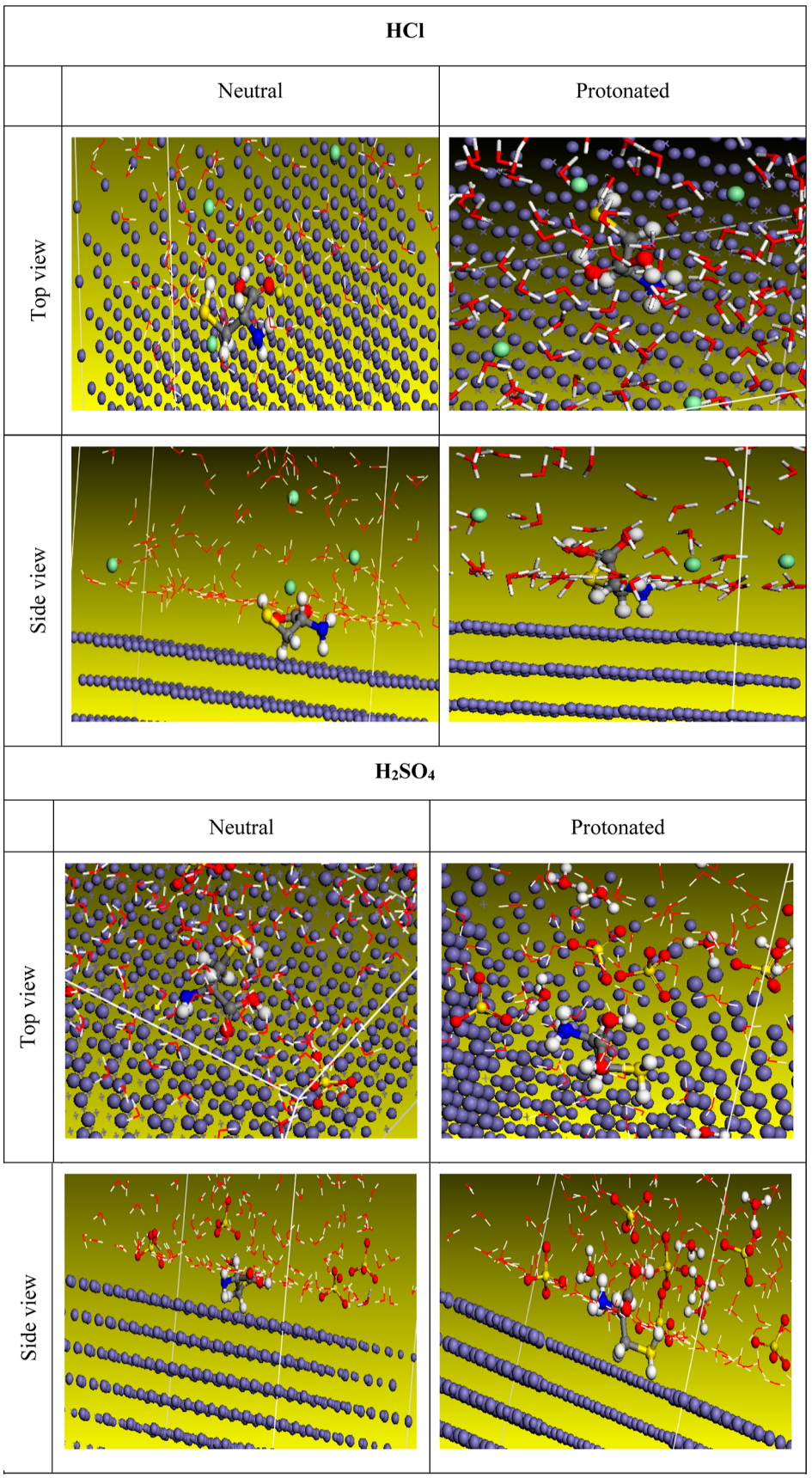

Figure 22. continued

https://doi.org/10.1021/acsomega.3c10522
ACS Omega 2024, 9, 13391−13411

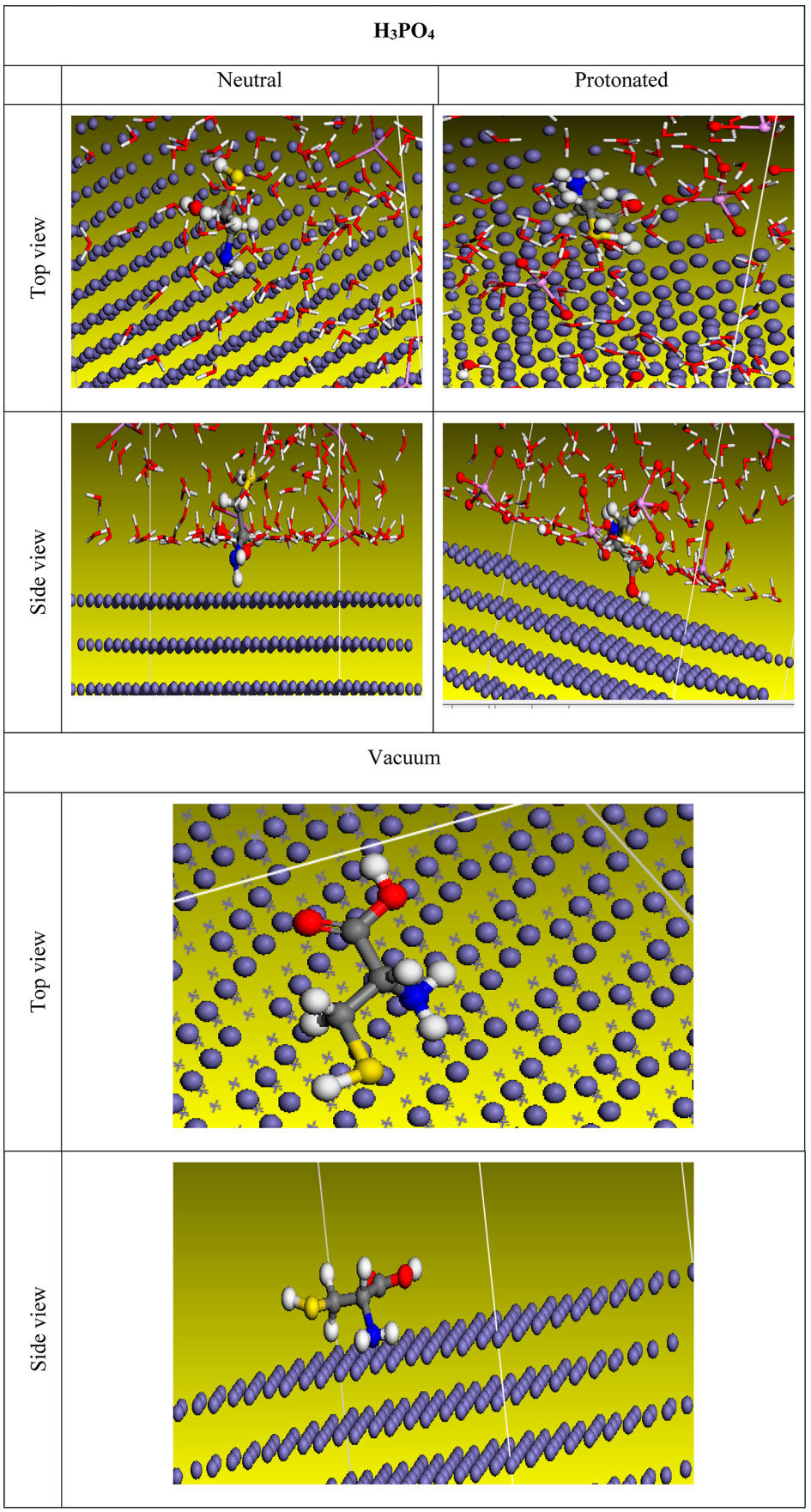

Figure 22. Most suited formation for adsorption of Cys. on carbo iron (110) substrate as determined by the adsorption locator module (neutral, protonated, and vacuum).

https://doi.org/10.1021/acsomega.3c10522
ACS Omega 2024, 9, 13391−13411

Table 6. Data and Specifications Obtained by Simulating Monte Carlo for Adsorption of Cys. on Iron (110) Substrate (Neutral, Protonated, and Vacuum)

factors	neutral	protonated
HCl		
total energy (kcal/mol)	−13148.10	−13223.60
adsorption energy (kcal/mol)	−6959.95	−6917.613
rigid adsorption energy (kcal/mol)	−7.14	−7371.680
deformation energy (kcal/mol)	184.63	454.07
dE_{ad}/dNi (kcal/mol)	−127.68	−156.24
H_2SO_4		
total energy (kcal/mol)	−4921.097	−4931.69
adsorption energy (kcal/mol)	−4954.22	−4941.09
deformation energy (kcal/mol)	−5131.816	−5120.76
rigid adsorption energy (kcal/mol)	177.59	179.67
dE_{ad}/dNi (kcal/mol)	−85.37	−128.12
H_3PO_4		
total energy (kcal/mol)	−7188.02	−7273.50
adsorption energy (kcal/mol)	−7221.17	−7282.91
rigid adsorption energy (kcal/mol)	−7471.02	−7535.37
deformation energy (kcal/mol)	249.85	252.46
dE_{ad}/dNi (kcal/mol)	−88.58	−191.14
Vacuum		
total energy (kcal/mol)	−34.12	
adsorption energy (kcal/mol)	−67.24	
rigid adsorption energy (kcal/mol)	−64.89	
deformation energy (kcal/mol)	−2.34	
dE_{ad}/dNi (kcal/mol)	−67.24	

simulation for the deformation, solid adsorption, and overall energies. By combining molecular energies from solid adsorption with deformation energies, the total energy (kcal mol^{-1}) computation for the substrate and Cys. is performed. When one of the adsorbate particles separates from the adsorbent substrate, the energy gained is measured in dE_{ads}/dNi (kcal mol^{-1}). In Table 6, we can see the Cys. adsorption energies. As demonstrated by the theoretical and applied research, it is very likely that the Cys. molecules are adsorbed on the surface of MSL, resulting in adsorbed layers that protect the surface against corrosion caused by the various acid solutions investigated. Table 6 and preceding studies[105,106] demonstrate the Cys. compound' successful operation in the solution (high adsorption energy). The local molecule's molecular structure is parallel to the surface, according to a detailed examination.[107,108] This adsorption pattern will be adopted by the retarding particle's constituent parts to enhance the metal's surface area or contact area. The enlarged metal/inhibitor contact zone will limit substrate access rather than triggering unwelcome chloride, sulfate, and phosphate anions assault.[107,108] It is projected that the electron transfer from the metallic surface to the Cys. compound will occur in reverse, reversing the process, when a charged proton component is present. Cys. molecules strongly adsorb on the MSL surface to form long-lasting adsorbent layers that shield the metal surface from several investigated acids that cause corrosion, as shown by theoretical and actual research (Table 6). In both a vacuum and an acidic (neutral and proton) environment, we investigated how molecules adsorb (Figure 22). The adsorption energies rise above the expected value in the presence of an aqueous solution, showing that Cys. molecules adsorb to the MSL surface more effectively (Table 6 for further details).

3.6. Inhibition Mechanism. The chemical composition, molecular size, and other pertinent factors like the functional groups, electron density, metal charge, and the nature of the corrosive medium all play a role in how much inhibition and interaction the Cys. molecules have with the MSL surface. Due to the unique structure of Cys. which contains $-NH_2$ group, −COOH, and −SH group, it adsorbs easily on the electrode surface. $-NH_2$ is the most basic group and therefore at pH < 7 it will be protonated. Thus, in acidic environments, the MSL surface is expected to be covered with a layer of anionic species (e.g., Cl^-, SO_4^{2-}, or PO_4^{-3}). As a result, electrostatic interaction occurs between the anionic species of acid and the protonated Cys. molecules at the electrolyte/metal interface. Accordingly, the anionic-protonated bridge provides the primary adsorption layer on the metal surface. Two important factors that affect the process are the strength of the acid and the number of corrosive species. The strongest acid here is HCl, followed by H_2SO_4, while H_3PO_4 is the weakest one. Hydrochloric acid is a stronger acid than H_2SO_4 because the H^+ dissociates more easily from the Cl^- than from the HSO_4^-. Thus, the degree of acid dissociation plays an important role in the protection of steel by Cys. Since HCl ionizes more completely and easier in one step compared to H_2SO_4 and H_3PO_4, it is expected that the protonation step of the inhibitor in HCl solution will be faster. As a result, Cys molecules in HCl solution adsorb quickly on the surface of MSL and so their inhibition capacity (% IE) in HCl is much higher than in other acids. Besides with the strength of the acid, in dilute solutions the number of the corrosive species like H^+, Cl^-, HSO_4^- and SO_4^{2-} is directly proportional to the corrosion rate. Thus, in the absence of Cys. since sulfuric acid is a strong diprotic acid, it can accelerate the corrosion rate of MSL more than monoprotic acid (HCl) and H_3PO_4 (being a weak acid). This means the order of corrosion strength (CR) of MSL in medium without Cys is H_2SO_4 > H_3PO_4 > HCl, while the order in the presence of Cys inhibitor (% IE) is the opposite (i.e., HCl > H_3PO_4> H_2SO_4). The molecules of the Cys. can bind to the surface of MSL in one of two behaviors: first, by moving the unshared pair electrons from oxygen, nitrogen, or sulfur atoms to the MSL's vacant d-orbital, which occurs in the anodic region and has a low energy. Second, by joining the molecules of the Cys. to the MSL's surface by a coordinating chemical connection. Bridges between the Cys. molecules and MSL are made using $(Fe\text{-}anion)_{ads}$ as a result of electrostatic attraction (physical adsorption) caused by the protonation of the Cys. molecules by chloride, phosphate, and sulfur anions. After that, the Cys. is adsorbed on the cathodic area to contest with hydrogen ions, producing cathode polarization to rise.[109] Third possibility is to occurrence of both chemical and physical interactions. Thus, it is necessary to estimate the zero-charge potential (ZCP), commonly known as the MSL surface charge at zero point. By applying the equation ($E_{corr} - E_q = 0$), the surface charge can be determined. Considering the data summarized in Table 1, the ZCP values are positive, and therefore the steel surface is positively charged.[46] Therefore, electrostatic repulsion occurs between the protonated Cys and the positively charged MSL surface. But as mentioned before, in acidic solutions, the MSL will be covered by anionic species causing an electrostatic interaction between the anionic species of acid and the protonated Cys molecules at the electrolyte/metal interface (physisorption). In addition, the estimated ΔG^0_{ads} value is about −40 kJ mol^{-1} (see Table 2), which indicates that the majority of adsorption is chemisorption.

https://doi.org/10.1021/acsomega.3c10522
ACS Omega 2024, 9, 13391−13411

4. CONCLUSIONS

Here, the nontoxic amino acid Cys. has been used as corrosion inhibitor for MSL in three different acidic media. Experimental results and simulation predictions have proven that it is a powerful inhibitor for corrosion protection of steel in harsh environments. The results showed that it behaves as a mixed-type inhibitor and follows the Langmuir adsorption model. By increasing the Cys. concentration and decreasing the temperature %, the IE increases. Due to the unique structure of Cys., adsorption studies have shown that it strongly and spontaneously adsorbs to the metal surface, forming a surface-protecting layer from corrosion. Cys. inhibits cathodic and anodic reactions, as determined by PDP methods. Increasing Cys. concentration results in a rise in R_{ct} and decreasing C_{dl}. Outcomes of SEM analysis for MSL with Cys.in HCl, H_3PO_4 and H_2SO_4 indicated that the steel surface was mores smoother in HCl, demonstrate the production of a protective film on the surface of MSL, which increases the effectiveness of inhibition. Electrochemical techniques, WL measurements, surface analysis, and quantum chemical calculations all were in agreement.

ASSOCIATED CONTENT

Supporting Information

The Supporting Information is available free of charge at https://pubs.acs.org/doi/10.1021/acsomega.3c10522.

WL measurements of MSL in 1 M HCl solution containing various concentrations of Cysteine after immersion time for 90 min at 25−55 °C. WL measurements of MSL in 1 M H_2SO_4 solution containing various concentrations of Cys. after immersion time for 90 min at 25−55 °C. WL measurements of MSL in 1 M H_3PO_4 solution containing various concentrations of Cysteine after immersion time for 90 min at 25−55°. Figures S1−S4 depict the WL of a MSL electrode dipped in a 1 M HCl solution containing various concentrations of Cysteine at 25−55 °C as a function of time. WL of a MSL electrode dipped in a 1 M H_2SO_4 solution containing various concentrations of Cysteine at 25−55 °C as a function of time. WL of a MSL electrode dipped in a 1 M H_3PO_4 solution containing various concentrations of Cysteine at 25−55 °C as a function of time. Plot of adsorption isotherms of Cysteine for corrosion of MSL in 3 acids, at different temperatures using WL method. Theoretical studies (PDF)

AUTHOR INFORMATION

Corresponding Authors

Hanaa. M. Elabbasy − *Misr Higher Institute for Engineering and Technology, Mansoura 35522, Egypt;* orcid.org/0000-0001-6779-6742; Email: helabbasy@hotmail.com

Arafat Toghan − *Chemistry Department, College of Science, Imam Mohammad Ibn Saud Islamic University (IMSIU), Riyadh 11623, Saudi Arabia; Chemistry Department, Faculty of Science, South Valley University, Qena 83523, Egypt;* orcid.org/0000-0002-1423-1147; Email: arafat.toghan@yahoo.com, aatahmed@imamu.edu.sa

Hend. S. Gadow − *Egypt High Institute of Engineering and Engineering and Technology, New Damietta 42519, Egypt;* orcid.org/0000-0002-4101-2441; Email: hsgado73@gmail.com

Complete contact information is available at: https://pubs.acs.org/10.1021/acsomega.3c10522

Notes

The authors declare no competing financial interest.

REFERENCES

(1) Toghan, A.; Fawzy, A. Unraveling the Adsorption mechanism and anti-corrosion functionality of dextrin and inulin as eco-friendly biopolymers for the corrosion of reinforced steel in 1.0 M HCl: A thermodynamic and kinetic approach. *Polymers* **2023**, *15*, 3144.

(2) Abd El-Lateef, H. M.; Shaaban, S.; Khalaf, M. M.; Toghan, A.; Shalabi, K. Synthesis, experimental, and computational studies of water soluble anthranilic organoselenium compounds as safe corrosion inhibitors for J55 pipeline steel in acidic oilfield formation water. *Colloids Surf., A* **2021**, *625*, 126894.

(3) Toghan, A.; Gadow, H.; Fawzy, A.; Alhussain, H.; Salah, H. Adsorption mechanism, Kinetics, Thermodynamics, and Anticorrosion Performance of a New Thiophene Derivative for C-steel in a 1.0 M HCl: Experimental and Computational approaches. *Metals* **2023**, *13*, 1565.

(4) Banerjee, G.; Malhotra, S. N. Contribution to Adsorption of Aromatic Amines on Mild Steel Surface from HCl Solutions by Impedance, UV, and Raman Spectroscopy. *Corrosion* **1992**, *48*, 10−15.

(5) Schmitt, G. Application of Inhibitors for Acid Media: Report prepared for the European Federation of Corrosion Working Party on Inhibitors. *Br. Corros. J.* **1984**, *19*, 165−176.

(6) Bijapur, K.; Molahalli, V.; Shetty, A.; Toghan, A.; De Padova, P.; Hegde, G. Recent trends and progress in corrosion inhibitors and electrochemical evaluation. *Appl. Sci.* **2023**, *13*, 10107.

(7) Toghan, A.; Fawzy, A.; Alakhras, A. I.; Farag, A. A. Electrochemical and theoretical examination of some imine compounds as corrosion inhibitors for carbon steel in oil wells formation water. *Int. J. Electrochem. Sci.* **2022**, *17*, 2212108.

(8) Farag, A.; Mohamed, E.; Toghan, A. The new trends in corrosion control using superhydrophobic surfaces: A review. *Corros. Rev.* **2023**, *41*, 21−37.

(9) Toghan, A.; Fawzy, A.; Al Bahir, A.; Alqarni, N.; Sanad, M.; Khairy, M.; Alakhras, A. I.; Farag, A. A. Computational foretelling and experimental implementation of the performance of polyacrylic acid and polyacrylamide polymers as eco-friendly corrosion inhibitors for copper in nitric acid. *Polymers* **2022**, *14*, 4802.

(10) Gadow, H. S.; Fawzy, A.; Khairy, M.; Sanad, M. M. S.; Toghan, A. Experimental and theoretical approaches to the inhibition of carbon steel corrosion by thiophene derivative in 1 M HCl. *Int. J. Electrochem. Sci.* **2023**, *18*, 100174.

(11) Toghan, A.; Khairy, M.; Huang, M.; Gadow, H. S. Electrochemical, surface analysis, and theoretical investigation of 3-hydroxy-5-(phenylamino)-4-(p-tolyldiazenyl)thiophen-2-yl)(phenyl)methanone as a corrosion inhibitor for carbon steel in a molar hydrochloric acid solution. *Int. J. Electrochem. Sci.* **2023**, *18*, 100070.

(12) Fawzy, A.; Toghan, A.; Alduaij, O. K.; Alqarni, N.; Eldesoky, A. M.; Farag, A. A. Electrochemical, spectroscopic, kinetic and surface analysis of the inhibitory performance of Alcian blue dye for copper corrosion in sulfuric acid solution. *Int. J. Electrochem. Sci.* **2024**, *19*, 100429.

(13) Toghan, A.; Fawzy, A.; Alakhras, A. I.; Sanad, M. M. S.; Khairy, M.; Farag, A. A. Correlating experimental with theoretical studies for a new ionic liquid for inhibiting corrosion of carbon steel during oil well acidification. *Metals* **2023**, *13*, 862.

(14) Toghan, A.; Khairy, M.; Huang, M.; Farag, A. A. Electrochemical, chemical and theoretical exploration of the corrosion inhibition of carbon steel with new imidazole-carboxamide derivatives in an acidic environment. *Int. J. Electrochem. Sci.* **2023**, *18*, 100072.

(15) Fawzy, A.; Toghan, A.; Alqarni, N.; Morad, M.; Zaki, M. E. A.; Sanad, M. M. S.; Alakhras, A. I.; Farag, A. A. Experimental and Computational Exploration of Chitin, Pectin, and Amylopectin Polymers as Efficient Eco-Friendly Corrosion Inhibitors for Mild

Steel in an Acidic Environment: Kinetic, Thermodynamic, and Mechanistic Aspects. *Polymers* **2023**, *15*, 891.
(16) Fawzy, A.; Al Bahir, A.; Alqarni, N.; Toghan, A.; Khider, M.; Ibrahim, I. M.; Abulreesh, H. H.; Elbanna, K. Evaluation of synthesized biosurfactants as promising corrosion inhibitors and alternative antibacterial and antidermatophytes agents. *Sci. Rep.* **2023**, *13*, 2585.
(17) Abd El-lateef, H. M.; El-Beltagi, H. S.; Mohamed Mohamed, M. E.; Kandeel, M.; Bakir, E.; Toghan, A.; Shalabi, K.; Tantawy, A. H.; Khalaf, M. M. Novel Natural Surfactant-Based Fatty Acids and Their Corrosion-Inhibitive Characteristics for Carbon Steel-Induced Sweet Corrosion: Detailed Practical and Computational Explorations. *Front. Mater. Sci.* **2022**, *9*, 843438.
(18) Toghan, A.; Fawzy, A.; Alqarni, N.; Abdelkader, A.; Alakhras, A. I. Inhibition Effects of Citrulline and Glutamine for Mild Steel Corrosion in Sulfuric Acid Environment: Thermodynamic and Kinetic Aspects. *Int. J. Electrochem. Sci.* **2021**, *16*, 211118.
(19) Toghan, A.; Gouda, M.; Shalabi, K.; El-Lateef, H. M. A. Preparation, characterization, and evaluation of macrocrystalline and nanocrystalline cellulose as potential corrosion inhibitors for ss316 alloy during acid pickling process: experimental and computational methods. *Polymers* **2021**, *13*, 2275.
(20) Fawzy, A.; Alsharief, H. H.; Toghan, A.; Bahir, A. A.; Alhasani, M.; Alqarni, N.; Alsaedi, A. M. R.; Fargaly, T. A. Evaluation of protection performances of novel synthesized bis-oxindole-based derivatives for the corrosion of aluminum in acidic environment. *J. Mol. Struct.* **2023**, *1294*, 136443.
(21) Fawzy, A.; Alduaij, O. K.; Al-Bahir, A.; Alshammari, D. A.; Alqarni, N.; Eldesoky, A. M.; Farag, A. A.; Toghan, A. A comparative study of pyridine and pyrimidine derivatives based formamidine for copper corrosion inhibition in nitric acid: Experimental and computational exploration. *Int. J. Electrochem. Sci.* **2024**, *19*, 100403.
(22) Chauhan, D. S.; Quraishi, M. A.; Srivastava, V.; Haque, J.; Ibrahimi, B. E. Virgin and chemically functionalized amino acids as green corrosion inhibitors: Influence of molecular structure through experimental and in silico studies. *J. Mol. Struct.* **2021**, *1226*, 129259.
(23) Pubchem. Chemical Information Database. 2022. Available online: https://pubchem.ncbi.nlm.nih.gov/ (accessed on August 10, 2022).
(24) Sigma Aldrich. L-Cys.-Material Safety Data Sheet. 2020. Available online: https://www.sigmaaldrich.com/CA/en/sds/aldrich/168149 (accessed on July 9, 2022).
(25) Thermo Fisher Scientific. *Material Safety Data Sheet*; Thermo Fisher Scientific: Waltham, MA, USA, 2021; Vol. 4, available online: https://us.vwr.com/assetsvc/asset/en_US/id/16490607/contents (accessed on 2 July, 2022).
(26) Amin, M. A.; Khaled, K. F.; Mohsen, Q.; Arida, H. A. A study of the inhibition of iron corrosion in HCl solutions by some amino acids. *Corros. Sci.* **2010**, *52*, 1684−1695.
(27) Morad, M. S. Effect of amino acids containing sulfur on the corrosion of mild steel in phosphoric acid solutions containing Cl−, F− and Fe3+ ions: Behavior under polarization conditions. *J. Appl. Electrochem.* **2005**, *35*, 889−895.
(28) Matos, J. B.; Pereira, L. P.; Agostinho, S. M. L.; Barcia, O. E.; Cordeiro, G. G. O.; D'Elia, E. Effect of cysteine on the anodic dissolution of copper in sulfuric acid medium. *J. Electroanal. Chem.* **2004**, *570*, 91−94.
(29) Morad, M. S. S.; Hermas, A. E.-H. A.; Aal, M. S. A. Effect of amino acids containing sulfur on the corrosion of mild steel in phosphoric acid solutions polluted with Cl^-, F^- and Fe^{3+} ions−behaviour near and at the corrosion potential. *J. Chem. Technol. Biotechnol.* **2002**, *77*, 486−494.
(30) Abdel-Fatah, H. T. M. The inhibition action of tyrosine on the corrosion of low chromium steel in 7 wt percent sulfamic acid. *Anti-Corros. Methods Mater.* **2012**, *59*, 23−31.
(31) Cang, H.; Fei, Z.; Shi, W.; Xu, Q. Experimental and Theoretical Study for Corrosion Inhibition of Mild Steel by L-Cysteine. *Int. J. Electrochem. Sci.* **2012**, *7*, 10121−10131.
(32) Fu, J.-J.; Li, S.-N.; Wang, Y.; Cao, L.-H.; Lu, L.-D. Computational and electrochemical studies of some amino acid compounds as corrosion inhibitors for mild steel in hydrochloric acid solution. *J. Mater. Sci.* **2010**, *45*, 6255−6265.
(33) Ozcan, M.; Karadağ, F.; Dehri, I. Interfacial Behavior of Cysteine between Mild Steel and Sulfuric Acid as Corrosion Inhibitor. *Acta Phys.-Chim. Sin.* **2008**, *24* (8), 1387−1392.
(34) El-Etre, A. Y. Natural onion juice as inhibitor for zinc corrosion. *Bull. Electrochem.* **2006**, *22*, 75−80.
(35) Kuruvilla, M.; John, S.; Joseph, A. Electrochemical studies on the interaction of l-cysteine with metallic copper in sulfuric acidL-cysteine with metallic copper in sulfuric acid. *Res. Chem. Intermed.* **2013**, *39*, 3531−3543.
(36) ASTM. *AST G 1−90, Standard Recommended Practice for the Laboratory Immersion Corrosion Testing of Metals*; American Society for Testing and Materials: Philadelphia, PA, USA, 1999.
(37) Bedair, M.; Metwally, M.; Soliman, S.; Al-Sabagh, A.; Salem, A.; Mohamed, T. Extracts of mint and tea as green corrosion inhibitors for MSL in hydrochloric acid solution. *Al-Azhar Bull. Sci.* **2015**, *26*, 1−14.
(38) Barsoukov, E.; Macdonald, J. R., *Impedance Spectroscopy, Theory, Experiment and Applications*, 2nd ed.; Wiley Inter-Science Publications: New York, 2005.
(39) Sheetal; Kundu, S.; Thakur, S.; Singh, A. K.; Singh, M.; Pani, B.; Saji, V. S. A Review of Electrochemical Techniques for Corrosion Monitoring - Fundamentals and Research Updates. *Crit. Rev. Anal. Chem.* **2023**, *25*, 1−26.
(40) Emori, W.; Zhang, R. H.; Okafor, P. C.; Zheng, X. W.; He, T.; Wei, K.; Lin, X. Z.; Cheng, C. R. Adsorption and corrosion inhibition performance of multi-phyto-constituents from Dioscorea septemloba on carbon steel in acidic media: characterization, experimental and theoretical studies. *Colloids Surf. A Physicochem. Eng. Asp.* **2020**, *590*, 124534.
(41) Abbas, M. A.; Bedair, M. A.; El-Azabawy, O. E.; Gad, E. S. Anticorrosion Effect of Ethoxylate Sulfanilamide Compounds on Carbon Steel in 1 M Hydrochloric Acid: Electrochemical and Theoretical Studies. *ACS Omega* **2021**, *6*, 15089−15102.
(42) Alarfaji, S. S.; Ali, I. H.; Bani-Fwaz, M. Z.; Bedair, M. A. Synthesis and Assessment of Two Malonyl Dihydrazide Derivatives as Corrosion Inhibitors for Carbon Steel in Acidic Media: Experimental and Theoretical Studies. *Molecules* **2021**, *26*, 3183.
(43) Heikal, M.; Ali, A.; Ibrahim, B. S.; Toghan, A. Electrochemical and physico-mechanical characterizations of fly ash-composite cement. *Constr. Build. Mater.* **2020**, *243*, 118309.
(44) Gadow, H. S.; Fakeeh, M. Green inhibitor of carbon steel corrosion in 1 M hydrochloric acid: Eruca sativa seed extract (experimental and theoretical studies). *RSC Adv.* **2022**, *12*, 8953−8986.
(45) Kokalj, A. On the HSAB based estimate of charge transfer between adsorbates and metal surfaces. *Chem. Phys.* **2012**, *393*, 1−12.
(46) Toghan, A.; Gadow, H. S.; Dardeer, H. M.; Elabbasy, H. M. New promising halogenated cyclic imides derivatives as potential corrosion inhibitors for carbon steel in hydrochloric acid solution. *J. Mol. Liq.* **2021**, *325*, 115136−115156.
(47) Elabbasy, H. M.; Gadow, H. S. Study the effect of expired tenoxicam on the inhibition of carbon steel corrosion in a solution of hydrochloric acid. *J. Mol. Liq.* **2021**, *321*, 114918−114935.
(48) Fawzy, A.; Toghan, A. Inhibition Evaluation of Chromotrope Dyes for the Corrosion of Mild Steel in an Acidic Environment: Thermodynamic and Kinetic Aspects. *ACS Omega* **2021**, *6*, 4051−4061.
(49) El-Etre, A. Y.; Abdallah, M. Natural honey as corrosion inhibitor for metals and alloys. II. C-steel in high saline water. *Corros. Sci.* **2000**, *42*, 731−738.
(50) Kaczerewska, O.; Leiva-Garcia, R.; Akid, R.; Brycki, B.; Kowalczyk, I.; Pospieszny, T. Effectiveness of O-bridged cationic gemini surfactants as corrosion inhibitors for stainless steel in 3 M HCl: experimental and theoretical studies. *J. Mol. Liq.* **2018**, *249*, 1113−1124.
(51) Bedair, M. A.; Soliman, S. A.; Metwally, M. S. Synthesis and characterization of some nonionic surfactants as corrosion inhibitors for steel in 1.0 M HCl (Experimental and computational study). *J. Ind. Eng. Chem.* **2016**, *41*, 10−22.

https://doi.org/10.1021/acsomega.3c10522
ACS Omega 2024, 9, 13391−13411

(52) Abdel Nazeer, A.; El-Abbasy, H. M.; Fouda, A. S. Antibacterial drugs as environmentally-friendly corrosion inhibitors for carbon steel in acid medium. *Res. Chem. Intermed.* **2013**, *39*, 921−939.
(53) Lgaz, H.; Salghi, R.; Subrahmanya Bhat, K.; Chaouiki, A.; Shubhalaxmi, S.; Jodeh, S. Correlated experimental and theoretical study on inhibition behavior of novel quinoline derivatives for the corrosion of mild steel in hydrochloric acid solution. *J. Mol. Liq.* **2017**, *244*, 154−168.
(54) Ramesh Saliyan, V.; Adhikari, A. V. Inhibition of corrosion of mild steel in acid media by N′-benzylidene-3-(quinolin-4-ylthio)-propanohydrazide. *Bull. Mater. Sci.* **2008**, *31*, 699−711.
(55) Bedair, M. A.; Soliman, S. A.; Bakr, M. F.; Gad, E. S.; Lgaz, H.; Chung, I.-M.; Salama, M.; Alqahtany, F. Z. Benzidine-based Schiff base compounds for employing as corrosion inhibitors for carbon steel in 1.0 M HCl aqueous media by chemical, electrochemical and computational methods. *J. Mol. Liq.* **2020**, *317*, 114015.
(56) Aljourani, J.; Golozar, M. A.; Raeissi, K. The inhibition of carbon steel corrosion in hydrochloric and sulfuric acid media using some benzimidazole derivatives. *Mater. Chem. Phys.* **2010**, *121*, 320−325.
(57) John, A. K. N. R.; Bockris, O. M. *Modern Electrochemistry1*; Springer: New York, NY, Boston, 1970.
(58) El-Sabbah, M. M. B.; Bedair, M. A.; Abbas, M. A.; Fahmy, A.; Hassaballa, S.; Moustafa, A. A. Synergistic effect between natural honey and 0.1 M KI as green corrosion inhibitor for steel in acid medium. *Z. Phys. Chem.* **2019**, *233*, 627−649.
(59) Wang, Q.; Liu, L.; Zhang, Q.; Wu, X.; Zheng, H.; Gao, P.; Zeng, G.; Yan, Z.; Sun, Y.; Li, Z.; Li, X. Insight into the anti-corrosion performance of Artemisia argyi leaves extract as eco-friendly corrosion inhibitor for carbon steel in HCl medium. *Sustainable Chem. Pharm.* **2022**, *27*, 100710.
(60) Bedair, M. A.; Soliman, S. A.; Hegazy, M. A.; Obot, I. B.; Ahmed, A. S. Empirical and theoretical investigations on the corrosion inhibition characteristics of mild steel by three new Schiff base derivatives. *J. Adhes. Sci. Technol.* **2019**, *33*, 1139−1168.
(61) Hamza, R. A.; Samawi, K. A.; Salman, T. A. Inhibition Studies of Aluminium Alloy (2024) Corrosion in Acid Hydrochloride Solution Using an Expired Phenylphrine Drug. *Egypt. J. Chem.* **2020**, *63*, 2863−2875.
(62) Santos, A. d. M.; Almeida, T. F.; Cotting, F.; Aoki, I. V.; Melo, H. G.; Capelossi, V. R. Evaluation of castor bark powder as a corrosion inhibitor for carbon steel in acidic media. *Mater. Res.* **2017**, *20*, 492−505.
(63) Idouhli, R.; N'Ait Ousidi, A.; Koumya, Y.; Abouelfida, A.; Benyaich, A.; Auhmani, A.; Ait Itto, M. Y. Electrochemical studies of monoterpenic thiosemicarbazones as corrosion inhibitor for steel in 1M HCl. *Int. J. Corros.* **2018**, *2018*, 1−15.
(64) Yadav, M.; Sharma, U.; Yadav, P. Corrosion inhibitive properties of some new isatin derivatives on corrosion of N80 steel in 15% HCl. *J. Ind. Chem.* **2013**, *4*, 6.
(65) Zhou, L.; Lv, Y.-L.; Hu, Y.-X.; Zhao, J.-H.; Xia, X.; Li, X. Experimental and theoretical investigations of 1,3,5-tris(4-aminophenoxy)benzene as an effective corrosion inhibitor for mild steel in 1 M HCl. *J. Mol. Liq.* **2018**, *249*, 179−187.
(66) Gadow, H.; Motawea, M. M.; Elabbasy, H. M. Investigation of myrrh extract as a new corrosion inhibitor for α-brass in 3.5% NaCl solution polluted by 16 ppm sulfide. *RSC Adv.* **2017**, *7*, 29883−29898.
(67) Zaher, A.; Chaouiki, A.; Salghi, R.; Boukhraz, A.; Bourkhiss, B.; Ouhssine, M. Inhibition of MSL corrosion in 1M hydrochloric medium by the Methanolic extract of Ammi visnaga L. lamseeds. *Int. J. Corros.* **2020**, *2020*, 9764206.
(68) Chen, J.; Qiang, Y.; Peng, S.; Gong, Z.; Zhang, S.; Gao, L.; Tan, B.; Chen, S.; Guo, L. Experimental and computational investigations of 2-amino-6-bromobenzothiazole as a corrosion inhibitor for copper in sulfuric acid. *J. Adhes. Sci. Technol.* **2018**, *32*, 2083−2098.
(69) Macdonald, D. D.; Mckubre, M. C. H. Impedance measurements in electrochemical systems. In *Modern Aspects of Electrochemistry 14*; Bockris, J. O'. M., Conway, B. E., White, R. E., Eds.; Plenum Press: New York, 1982; p 61.
(70) Ali, S. M.; Al Lehaibi, H. A. Control of zinc corrosion in acidic media: Green fenugreek inhibitor. *Trans. Nonferrous Met. Soc. China* **2016**, *26*, 3034−3045.
(71) Galai, M.; Benqlilou, H.; Touhami, M. E.; Belhaj, T.; Berrami, K.; Kafssaoui, H. E. Comparative analysis for the corrosion susceptibility of copper alloys in sandy soil. *Environ. Eng. Res.* **2018**, *23* (2), 164−174.
(72) Outirite, M.; Lagrenee, M.; Lebrini, M.; Traisnel, M.; Jama, C.; Vezin, H.; Bentiss, F. Ac impedance, X-ray photoelectron spectroscopy and density functional theory studies of 3,5-bis(n-pyridyl)-1,2,4-oxadiazoles as efficient corrosion inhibitors for carbon steel surface in hydrochloric acid solution. *Electrochim. Acta* **2010**, *55*, 1670−1681.
(73) Muthukrishnan, P.; Prakash, P.; Jeyaprabha, B.; Shankar, K. Stigmasterol extracted from Ficus hispida leaves as a green inhibitor for the mild steel corrosion in 1 M HCl solution. *Arab. J. Chem.* **2019**, *12*, 3345−3356.
(74) Mo, S.; Qin, T. T.; Luo, H. Q.; Li, N. B. Insights into the corrosion inhibition of copper in hydrochloric acid solution by self-assembled films of 4-octylphenol. *RSC Adv.* **2015**, *5*, 90542−90549.
(75) Chen, W.; Hong, S.; Xiang, B.; Luo, H.; Li, M.; Li, N. Corrosion inhibition of copper in hydrochloric acid by coverage with trithiocyanuric acid self-assembled monolayers. *Corros. Eng., Sci. Technol.* **2013**, *48*, 98−107.
(76) Habeeb, H. J.; Luaibi, H. M.; Dakhil, R. M.; Kadhum, A. A. H.; Al-Amiery, A. A.; Gaaz, T. S. Development of new corrosion inhibitor tested on mild steel supported by electrochemical study. *Results Phys.* **2018**, *8*, 1260−1267.
(77) Kumari, P. P.; Shetty, P.; Rao, S. A. Electrochemical measurements for the corrosion inhibition of MSL in 1 M hydrochloric acid by using an aromatic hydrazide derivative. *Arab. J. Chem.* **2017**, *10*, 653−663.
(78) Volpi, E.; Foiadelli, C.; Trasatti, S.; Koleva, D. A. Development of smart corrosion inhibitors for reinforced concrete structures exposed to a microbial environment. *Ind. Eng. Chem. Res.* **2017**, *56*, 5778−5794.
(79) Ali, I. H.; Suleiman, M. H. A. Effect of Acid extract of leaves of juniperus procera on corrosion inhibition of carbon steel in HCl solutions. *Int. J. Electrochem. Sci.* **2018**, *13*, 3910−3922.
(80) Idusuyi, N.; Ajide, O. O.; Oluwole, O. O.; Arotiba, O. A. Electrochemical impedance study of an Al6063−12%SiC-Cr composite immersed in 3 wt.% sodium chloride. *Procedia Manuf.* **2017**, *7*, 413−419.
(81) Mohan, R.; Joseph, A. Corrosion protection of mild steel in hydrochloric acid up to 313 K using propyl benzimidazole: Electro-analytical, adsorption and quantum chemical studies. *Egypt. J. Pet.* **2018**, *27*, 11−20.
(82) Benabdellah, M.; Tounsi, A.; Khaled, K. F.; Hammouti, B. Thermodynamic, chemical and electrochemical investigations of 2-mercapto benzimidazole as corrosion inhibitor for mild steel in hydrochloric acid solutions. *Arab. J. Chem.* **2011**, *4*, 17−24.
(83) Zheng, X.; Gong, M.; Li, Q.; Guo, L. Corrosion inhibition of mild steel in sulfuric acid solution by loquat (Eriobotrya japonica Lindl.) leaves extract. *Sci. Rep.* **2018**, *8*, 9140.
(84) Yurt, A.; Bereket, G.; Kivrak, A.; Balaban, A.; Erk, B. Effect of Schiff Bases Containing Pyridyl Group as Corrosion Inhibitors for Low Carbon Steel in 0.1 M HCl. *J. Appl. Electrochem.* **2005**, *35*, 1025−1032.
(85) Saliyan, V. R.; Adhikari, A. V. Quinolin-5-ylmethylene-3-{[8-(trifluoromethyl)quinolin-4-yl]thio}propanohydrazide as an effective inhibitor of mild steel corrosion in HCl solution. *Corros. Sci.* **2008**, *50*, 55−61.
(86) Fekry, A. M.; Mohamed, R. R. Acetyl thiourea chitosan as an eco-friendly inhibitor for mild steel in sulphuric acid medium. *Electrochim. Acta* **2010**, *55*, 1933−1939.
(87) Fouda, A. S.; Mohamed, O. A.; Elabbasy, H. M. Ferula hermonis Plant Extract as Safe Corrosion Inhibitor for Zinc in Hydrochloric Acid Solution. *J. Bio-Tribo-Corros.* **2021**, *7*, 135.
(88) Honarvar Nazari, M.; Shihab, M. S.; Havens, E. A.; Shi, X. Mechanism of corrosion protection in chloride solutionby an apple-based green inhibitor: experimental and theoretical studies. *J. Infrastruct. Preserv. Resilience* **2020**, *1*, 7−25.

https://doi.org/10.1021/acsomega.3c10522
ACS Omega 2024, 9, 13391−13411

(89) Kacimi, Y. E.; Touir, R.; Alaoui, K.; Kaya, S.; Abousalem, A. S.; Ouakki, M.; Touhami, M. E. Anti-corrosion properties of 2-Phenyl-4(3H)-quinazolinone-substituted compounds: electrochemical, quantum chemical, Monte Carlo, and molecular dynamic simulation investigation. *J. Bio- Tribo-Corros.* **2020**, *6*, 47−71.
(90) Koumya, Y.; Idouhli, R.; Oukhrib, A.; Khadiri, M.; Abouelfida, A.; Benyaich, A. Synthesis, electrochemical, thermodynamic, and quantum chemical investigations of amino Cadalene as a corrosion inhibitor for stainless steel type 321 in sulfuric acid 1M. *Int. J. Electrochem.* **2020**, *2020*, 5620530−5620540.
(91) Danaee, I.; RameshKumar, S.; RashvandAvei, M.; Vijayan, M. Electrochemical and Quantum Chemical Studies on Corrosion Inhibition Performance of 2,2'-(2-Hydroxyethylimino)bis[N-(alphaalpha-dimethylphenethyl)-N-methylacetamide] on Mild Steel Corrosion in 1M HCl Solution. *Mater. Res.* **2020**, *23*, No. e20180610.
(92) Obot, I. B.; Obi-Egbedi, N. O. Indeno-1-one [2,3-b]quinoxaline as an effective inhibitor for the corrosion of MSL in 0.5M H_2SO_4 solution. *Mater. Chem. Phys.* **2010**, *122*, 325−328.
(93) Mert, B. D.; Erman Mert, M.; Kardas, G.; Yazici, B. Experimental and theoretical investigation of 3-amino-1,2, 4-triazole-5-thiol as a corrosion inhibitor for carbon steel in HCl medium. *Corros. Sci.* **2011**, *53*, 4265−4272.
(94) Gece, G. The use of quantum chemical methods in corrosion inhibitor studies. *Corros. Sci.* **2008**, *50*, 2981−2992.
(95) Ansari, K. R.; Ramkumar, S.; Nalini, D.; Quraishi, M. A. Studies on adsorption and corrosion inhibitive properties of quinoline derivatives on N80 steel in 15% hydrochloric acid. *Cogent Chem.* **2016**, *2*, 1145032−1145045.
(96) Mathew, Z. P.; Rajan, K.; Augustine, C.; Joseph, B.; John, S. Corrosion inhibition of mild steel using poly (2-ethyl -2-oxazoline) in 0.1M HCl solution. *Heliyon* **2020**, *6*, No. e05560.
(97) Hoai Vu, N. S.; Hien, P. V.; Mathesh, M.; Hanh Thu, V. T.; Nam, N. D. Improved Corrosion Resistance of Steel in Ethanol Fuel Blend by Titania Nanoparticles and Aganonerion polymorphum Leaf Extract. *ACS Omega* **2019**, *4*, 146−158.
(98) Lukovits, I.; Kálmán, E.; Zucchi, F. Corrosion Inhibitors—Correlation between Electronic Structure and Efficiency. *Corrosion* **2001**, *57*, 3−8.
(99) Zhang, W.; Liu, Y.; Zhang, Y.; Wang, L. J.; Wu, Y.-C.; Li, H.-J. 9-Substituted acridines as effective corrosion inhibitors for mild steel: electrochemical, surface morphology, and computational studies. *New J. Chem.* **2020**, *44*, 6464−6474.
(100) Boughoues, Y.; Benamira, M.; Messaadia, L.; Bouider, N.; Abdelaziz, S. Experimental and theoretical investigations of four amine derivatives as effective corrosion inhibitors for mild steel in HCl medium. *RSC Adv.* **2020**, *10*, 24145−24158.
(101) Bedair, M. A. The effect of structure parameters on the corrosion inhibition effect of some heterocyclic nitrogen organic compounds. *J. Mol. Liq.* **2016**, *219*, 128−141.
(102) Abdelshafi, N. S.; Ibrahim, M. A.; Badran, A. S.; Halim, S. A. Experimental and theoretical evaluation of a newly synthesized quinoline derivative as corrosion inhibitor for iron in 1.0 M hydrochloric acid solution. *J. Mol. Struct.* **2022**, *1250*, 131750.
(103) Shalabi, K.; Abdallah, Y. M.; Hassan, H. M.; Fouda, A. S. Adsorption and Corrosion Inhibition of Atropa Belladonna Extract on Carbon Steel in 1 M HCl Solution. *Int. J. Electrochem. Sci.* **2014**, *9*, 1468−1487.
(104) Roque, J. M.; Pandiyan, T.; Cruz, J.; García-Ochoa, E. DFT and electrochemical studies of tris(benzimidazole-2-ylmethyl)amine as an efficient corrosion inhibitor for carbon steel surface. *Corros. Sci.* **2008**, *50*, 614−624.
(105) Dagdag, O.; Safi, Z.; Erramli, H.; Cherkaoui, O.; Wazzan, N.; Guo, L.; Verma, C.; Ebenso, E.; El Harfi, A. Adsorption and anticorrosive behavior of aromatic epoxy monomers on carbon steel corrosion in acidic solution: computational studies and sustained experimental studies. *RSC Adv.* **2019**, *9*, 14782−14796.
(106) Qiang, Y.; Zhang, S.; Xu, S.; Li, W. Experimental and theoretical studies on the corrosion inhibition of copper by two indazole derivatives in 3.0% NaCl solution. *J. Colloid Interface Sci.* **2016**, *472*, 52−59.
(107) Qiang, Y.; Zhang, S.; Guo, L.; Xu, S.; Feng, L.; Obot, I. B.; Chen, S. Sodium dodecyl benzene sulfonate as a sustainable inhibitor for zinc corrosion in 26% NH_4Cl solution. *J. Clean. Prod.* **2017**, *152*, 17−25.
(108) Ahmed, S. K.; Ali, W. B.; Khadom, A. A. Synthesis and investigations of heterocyclic compounds as corrosion inhibitors for mild steel in hydrochloric acid. *Int. J. Ind. Chem.* **2019**, *10*, 159−173.
(109) Biswas, A.; Pal, S.; Udayabhanu, G. Experimental and theoretical studies of xanthan gum and its graft co-polymer as corrosion inhibitor for mild steel in 15% HCl. *Appl. Surf. Sci.* **2015**, *353*, 173−183.

https://doi.org/10.1021/acsomega.3c10522
ACS Omega 2024, 9, 13391−13411